Master’s Thesis

Master’s degree in Electronic Engineering (MEE)

Experimental monitoring of the gain in RF Power Amplifiers using Temperature Measurements

MEMORY

May 19, 2022

Autor: Xavier Gisbert Beguer

Directors: Diego Mateo Peña and Josep Altet Sanahujes

Convocatory: May 24, 2022

Escola Tècnica Superior
d’Enginyeria de Telecomunicació de Barcelona

Abstract

The Aging effect is intrinsic to transistors in integrated circuits and occurs sooner with newer, smaller manufacturing node technologies. With prolonged usage within the nominal power and biasing operating point, some charges get trapped in the transistor channel and carrier mobility is reduced, the threshold voltage V_T is increased and operating point changes, decreasing the drain current I_D and gain. This results in worsened DC and RF characteristics of the transistor in a power amplifier PA, and so are their precision or communication power in analog or RF applications, respectively. The Aging can be calibrated and corrected by modifying the biasing, restoring the original gain at the cost of increased power consumption.

To this date, this recalibration is performed with integrated power sensors that monitor the gain and control it by modifying the biasing. This method, however, uses valuable layout space and is a direct measurement which modifies the real circuit topology, having an impact on its characteristics and behavior.

Prior research in the ETSETB Electronics Engineering department proposed the usage of temperature measurements, indirect by nature so they do not modify the circuit topology, to control the gain by also modifying the biasing as the Aging progresses. The studies proposed heterodyne (two RF tones) over homodyne (one RF tone) temperature measurements as being less prone to noise. An IC to test this principles called PAAGEANT was designed, simulated and manufactured, and 20 ICs are available at the ETSETB Electronics laboratory.

This thesis experimentally characterizes in DC and RF one PA in the PAAGEANT IC to extract its gain and characterizes its temperature sensor TS and thermal coupling between the PA and TS. These characteristics are used to then propose experimental signatures relating the gain and temperature measurements. Several methods of temperature measurement of the PA are tested and studied with 11 ICs to ensure repeatability. In further studies, the signatures will be measured during and after the aging process, so a control system modifying the biasing can correct the resulting temperature signature of each IC after Aging to the signature measured before Aging, and so will the gain.

Some temperature sensor TS characteristics vary among the measured ICs, and results show that the signatures must be calibrated for individual manufactured ICs. The homodyne and heterodyne signatures proposed in this Master's Thesis show promise in being used in control systems that will be correcting the gain-temperature signatures.

Contents

1 Preface 9

2 Introduction 11
2.1 Objectives . . . 11
2.2 Scope of the thesis . . . 12
2.3 Sections . . . 12
2.4 Keywords . . . 12

3 Theory Frame 15
3.1 Direct and indirect measurements . . . 15
3.2 Need of gain signatures . . . 15
3.3 Temperature in RF power amplifiers . . . 15
3.3.1 Temperature sensor . . . 15
3.3.2 Thermal coupling . . . 16
3.3.2.1 Power dissipated by the input resistor R_{bias} . . . 17
3.3.2.2 Power dissipated subfolding . . . 17
3.3.3 Homodyne temperature measurements . . . 17
3.3.4 Heterodyne temperature measurements . . . 19

4 Implementation 21
4.1 PAAGEANT Chip . . . 21
4.1.1 Differential temperature sensors in PAAGEANT . . . 22
4.1.2 Different sensor configurations in PAs . . . 23
4.1.2.1 PA 1 . . . 23
4.1.2.2 PA 2 . . . 23
4.1.2.3 PA 3 . . . 24
4.2 Instruments used in the measurements . . . 24
4.3 Code . . . 24
4.3.1 A0Y: DC and RF characterization of the PA . . . 26
4.3.1.1 A03: AC frequency response . . . 26
4.3.1.2 A04: 1dB compression point with f_s. . . . 26
4.3.1.3 A05: RF gain characteristics . . . 26
4.3.1.4 A06: I_D characterization to V_{GS} and V_{DS} . . . 26
4.3.2 BXY: Homodyne, TS sensor and thermal coupling characterization and gain signatures . . . 26
4.3.2.1 BX1: TS non-bias voltage-temperature curve . . . 26
4.3.2.2 BX2: TS bias voltage-temperature curve and TS sensitivity and dynamic range. . . . 26
4.3.2.3 BX3: TS voltage-temperature curve for non-bias, bias and bias with input RF signal . . . 26
4.3.2.4 BX5: Signature 2 (2a and 2b) . . . 26
4.3.2.5 BX6: Thermal coupling from biasing . . . 26
4.3.2.6 BX7: Thermal coupling from $P_{R_{IN}}$ . . . 26
4.3.2.7 BX8: Signature 1 . . . 27
4.3.3 CXY: Heterodyne temperature characterization and gain signatures . . . 27
4.3.3.1 CX4: Signatures 3 and 4 . . . 27
4.3.4 DX1: S Parameters characterization . . . 27

telecos BCN

4.3.5 E01: Convert data . . . 27
4.3.6 E02: Plot figures . . . 27
4.3.7 E03: Post-process all ICs signatures and characteristics . . . 27

5 Measurements 29
5.1 Power Amplifier characterization . . . 29
5.2 Quantifying thermal coupling . . . 32
5.2.1 Temperature Sensor characterization . . . 32
5.2.1.1 Sensitivity and Dynamic Range . . . 32
5.2.2 DC thermal coupling . . . 34
5.2.2.1 DC thermal coupling due to the bias point . . . 35
5.2.2.2 DC thermal coupling due to the input resistor R_{bias} . . . 36
5.3 Gain signatures . . . 36
5.3.1 Homodyne gain signatures . . . 36
5.3.1.1 Signature 1: $Gain(\Delta V_{OUT_{DC}}); V_{OUT_{TS}}@P_{IN} = [-20, -10]dBm$. 37
5.3.1.2 Signature 2a: $Gain(\Delta N);\ N@P_{IN} = [-5, 5]dBm$ . . . 39
5.3.1.3 Signature 2b: $Gain(\Delta N)$ and $I_D(\Delta N);\ N@P_{IN} = [OFF, -20]dBm$ 40
5.3.2 Heterodyne gain signatures . . . 41
5.3.2.1 Signature 3: $Gain(slope\ log(V_{OUT_{TS}Lock-in}) - kP_{IN})$ . . . 42
5.3.2.2 Signature 4: $P_{OUT}(slope\ log(V_{OUT_{TS}Lock-in}) - kP_{IN},);\ N@P_{IN} = [OFF, -20dBm]$ . . . 43
5.4 Conclusions on the proposed gain signatures . . . 44

Conclusions 47

Acknowledgements 49

Bibliography 51

List of Figures

1 Circuital model of the thermal coupling mechanism, extracted from Figure 2 in [2]. 16
2 Example of thermal coupling. Normalized frequency response. CUT is a MOS transistor (dimensions: W = 100 μm, L = 10 μm) at a 25 μm distance from the temperature transducer. Extracted from [3]. 16
3 Layout of a PA and its TS in the IC PAAGEANT. Orange marks the reference transistor at the PA biasing, red marks the R_{bias} separating the DC biasing and RF input and blue marks the PA transistor. 17
4 Description of the physical mechanisms that take place in built-in homodyne temperature measurements: a) a linear CUT and a temperature sensor are placed in the same silicon die, c) spectral components of the CUT electrical signals, power dissipated by the CUT and temperature at the transducer location with homodyne excitation. Extracted from Figure 2 in [2]. 18
5 Description of the physical mechanisms that take place in built-in heterodyne temperature measurements: d) heterodyne CUT excitation, and e) spectral components under heterodyne CUT excitation. Extracted from Figure 2 in [2]. 19
6 Layout of the PAAGEANT IC. 21
7 PAAGEANT IC block layout, extracted from [4]. 21
8 Temperature sensor biasing structure (simplified) of the PAAGEANT IC. 21
9 Typical characteristic curve of the core temperature sensor. Extracted from Figure 4 in [1]. 22
10 Characteristic curve of the differential temperature sensor with an extended dynamic range. Extracted from Figure 5 in [1]. 22
11 Schematic of the core circuit of the temperature sensor with current bleeding for extended dynamic range and variability compensation. Transistor Q1 is placed by the CUT and away from Q2 and the rest of the sensor. Extracted from Figure 6 in [1]. 22
12 Scheme of the 10-bit current-steering DAC designed for the implementation of the bleeding current $I_{BLEED}(n)$, based on unary-weighted current sources. Extracted from Figure 13 in [1]. 22
13 PA schematic in the PAAGEANT IC. 23
14 Connections diagram of the PCB and instrumentation. 24
15 Laboratory setup. 25
16 Drain current $I_{D_{DC}}$ characteristics vs V_{GS} of PA 1. $V_T = 0.05V$ is observed. 29
17 Drain current $I_{D_{DC}}$ characteristics vs V_{DS} of PA 1. 29
18 Gain characteristics for f_s of PA 1. 30
19 Drain current $I_{D_{DC}}$ characteristics for f_s of PA 1. 30
20 S parameters of PA 1. 30
21 1dB compression points of PA 1 around the operating frequency $f_s = 170MHz$. . . 31
22 AC characteristics of PA 1 for different V_{GS}. 32
23 $V_{OUT_{TS}}$ vs TS DAC (N) sweep for different V_{SEN1b} bias voltages for the PA non-biased (dashed line) and biased (solid line) in Chip 30. 33
24 $V_{OUT_{TS}}$ vs TS DAC (N) sweep for different V_{SEN1b} bias voltages for the PA non-biased (dashed line) and biased (solid line) in Chip 22. 33
25 Non-biased sensitivity comparison for TS 1 (PA 1). 34
26 Biased sensitivity comparison for TS 1 (PA 1). 34
27 Non-biased dynamic range comparison for TS 1 (PA 1). 35

28 Biased dynamic range comparison for TS 1 (PA 1). 35
29 DC thermal coupling due to the gate-source bias point of PA 1. The different points correspond to values of $V_{GS} = [0.74, 0.79, 0.84, 0.89, 0.94, 0.99, 1.04]V$. 36
30 DC thermal coupling due to the drain-source bias point of PA 1. The different points correspond to values of $V_{GS} = [0.74, 0.79, 0.84, 0.89, 0.94, 0.99, 1.04]V$. 36
31 Temperature sensor output voltage $V_{OUT_{TS}}$ (top) for fixed N (bottom) used in Signature 1 of TS 1 (PA 1), measured at $P_{IN} = [-20, -10]dBm$ for chip 22. 37
32 Signature 1 of TS 1 (PA 1), measured at $P_{IN} = [-20, -10]dBm$ for chip 22. 38
33 Shape of the linear fitting of Signature 1 for different values of right P_{IN} with left $P_{IN} = -20dBm$ for TS 1 (PA 1). 38
34 Comparison of linear fitting of Signature 1 of TS 1 (PA 1) for 11 ICs. 39
35 Coefficients of polynomial fitting of proposed Signature 1 of TS 1 (PA 1) for 11 ICs. 39
36 Features used in Signatures 2a and 2b of TS 1 (PA 1) for IC 22, measured at $P_{IN} = [-5, 5]$ dB. 40
37 Signature 2a of TS 1 (PA 1) for IC 22. 40
38 Comparison of polynomial fitting of Signature 2a of TS 1 (PA 1) for 11 ICs. 40
39 Proposed Signature 2a for TS 1 (PA 1). 40
40 Scatter plot and polynomial fitting Signature 2b $Gain(\Delta N)$ and $I_D(\Delta N)$; $N@P_{IN} = [OFF, -20dBm]$ for TS 1 (PA 1) for IC 22. 41
41 Comparison of polynomial fittings of Signature 2b for TS 1 (PA 1) for 11 ICs. . . 41
42 Coefficients of polynomial fitting of proposed Signature 2b $Gain(\Delta N)$; $N@P_{IN} = [OFF, -20dBm]$ of TS 1 (PA 1) for 11 ICs. 41
43 Coefficients of polynomial fitting of proposed Signature 2b $I_D(\Delta N)$; $N@P_{IN} = [OFF, -20dBm]$ of TS 1 (PA 1) for 11 ICs. 41
44 Heterodyne characteristics $V_{OUT_{TS}Lock-in}(Gain)$ for different P_{IN} of TS 1 (PA 1) for IC 22. 42
45 Heterodyne characteristics $V_{OUT_{TS}Lock-in}(Gain)$ for different V_{GS} of TS 1 (PA 1) for IC 22. 42
46 Scatter plot and polynomial fitting of Signature 3 of TS 1 (PA 1) for IC 22. 43
47 Proposed Signature 3 ranges of TS 1 (PA 1) for IC 22. 43
48 Comparison of polynomial fittings of Signature 3 of TS 1 (PA 1) for 11 ICs. 43
49 Coefficients of polynomial fitting of proposed Signature 3 of TS 1 (PA 1) for 11 ICs. 43
50 Signature 4 of TS 1 (PA 1) for IC 22. 44

List of Tables

1 Sensor configurations of the different PAs in the PAAGEANT IC. 23
2 Instruments used to bias and measure the PAAGEANT IC. 25
3 TS 1 (PA 1) characteristics for 11 chips measured. mW/N values only measured for chosen $V_{SEN1b} = 2.5V$ at section **??**. 34
4 TS 1 (PA 1) thermal coupling for 11 chips measured. 35
5 Fitting parameters of the TS 1 (PA 1) signatures for 11 chips measured. 45

1 Preface

This Master's Thesis was done as part of an effort to empirically demonstrate the thermal calibration for aging technique proposed by Josep Altet, Diego Mateo, et al. as part of the TOGETHER national research project.

The PAAGEANT IC was developed and manufactured to test and validate the proposed methods. It consists of 3 PAs, with different configurations of integrated temperature and power sensors. 20 copies of the PAAGEANT IC, a PCB to connect and operate the IC and a set of laboratory instruments were given at the beginning of the thesis. MATLAB code, consisting of classes that connect and drive the instruments and previous students' programs, were also given at the start of the thesis. Other studies have previously simulated the characteristics of the PA in PAAGEANT, and some experimental measurements were performed.

This thesis has focused on experimentally characterizing the PA and temperature measurement with 11 ICs measured, and doing so with programs that operate in a very structured and automatic way so that the measurements can be later post-processed and the programs reused for further research.

Signatures are proposed that relate temperature measurements to gain characteristics, and can be calibrated to individual manufactured ICs. After the PA suffers Aging its DC and RF characteristics will be modified losing gain, so the temperature measurements conforming its signatures will have changed as well. Control systems using the temperature measurements and modifying the biasing can be made that attempt to restore the original temperature signature, and with it the gain will be corrected to the original value.

2 Introduction

Electronics and communications technologies benefit from the ever-increasing advancements in technology scaling. Smaller, more efficient and better performing silicon manufacturing processes have not only favored digital electronics, but also analog and RF. The improved procedures and technologies become cheaper and allow for more compact, complex and energy efficient designs.

One side effect of the silicon manufacturing nodes shrinking is the acceleration of an unwanted process known as Aging. Over time and use under nominal biasing, some charges get trapped in transistor channel and carrier mobility is reduced. This increases the threshold voltage V_T, changing the characteristics of the transistor. In a circuit, this means that drain current I_D and gain decrease, and precision or communication power are worsened. The Aging can be calibrated and corrected by modifying the biasing, restoring the original gain at the cost of increased power consumption.

Aging is present in all transistor nodes, and the *long* nodes in use decades ago became significant after about 20 years of use. What were acceptable circuit lifetimes in the earlier processes is coming closer to 5 and 3 years of usage in the recent *shorter* manufacturing nodes.

It is already common practice to correct Aging in sensitive circuits by introducing integrated power sensors that perform gain monitoring and control it by modifying the biasing. The power sensors are, however, a direct measurement that modifies the topology of the circuit measured and uses up valuable layout space in the IC.

[1] and [2] propose using embedded temperature sensors to characterize RF analog circuits. Integrated temperature sensors are indirect measurements, so the circuit topology is preserved, they require very little space in the IC layout and their implementation does not need to be sophisticated.

To this aim, as part of the TOGETHER national research project an IC called PAAGEANT has been designed, manufactured, simulated and tested. PAAGEANT contains 3 PAs, 2 temperature sensors and 2 power sensors and necessary to demonstrate the methodologies proposed to recalibrate power amplifiers after they have suffered aging by using temperature measurements.

This thesis aims to characterize in DC and RF the PA, characterize the TS and thermal coupling and propose and experimentally study several homodyne and heterodyne temperature-gain signatures. The signatures quantify experimental relations between temperature measurements and gain in each manufactured IC.

Several signatures using different measurement methods are proposed in this thesis, so that control systems can be devised that modify the PA biasing to correct the Aging suffered by using the temperature measurements forming the signatures before and after the Aging process. Automated MATLAB programs have been developed that perform the PA and temperature characterization and the temperature-gain signatures, and experimental results from 11 ICs are studied in this Master's Thesis to ensure repeatability.

2.1 Objectives

- Experimentally study the DC characteristics of the power amplifier PA

- Experimentally study the RF characteristics of the power amplifier PA
- Experimentally study the characteristics of the temperature sensor TS
- Experimentally study the thermal coupling between the power amplifier PA and temperature sensor TS, built in the same silicon die
- Propose and experimentally study signatures that relate the temperature measurements and gain characteristics of the PA
- Experimentally measure the above characteristics and signatures for 11 ICs to study their repeatability

2.2 Scope of the thesis

The present thesis will achieve the above objectives for TS 1 and PA 1. The temperature-gain signatures will use the many variables of temperature measurement, to have a variety of experimental options. From a maximum of 20 chips available, at least half of this amount must be measured.

2.3 Sections

This memory will first present the theory frame on temperature in RF power amplifiers in Section 3, detailing the homodyne and heterodyne methodologies available. Then the PAAGEANT IC used in the laboratory will be presented in Section 4, along with the instruments and programs developed. Finally, the measurements of the power amplifier DC and RF characterization, temperature sensor characteristics, thermal coupling and signatures will be presented in Section 5.

2.4 Keywords

- *PA*: Power amplifier
- *TS*: Temperature sensor
- *PS*: Power sensor
- *IC*: Integrated circuit
- *CUT*: Circuit under test
- *PAAGEANT*: Integrated circuit used in this thesis, detailed in Section 4.1
- *Signature*: Experimental relation between two magnitudes, like temperature and gain. Signatures developed in this thesis consist of temperature measurements, such as variation of TS DC output voltage $V_{OUT_{TS}}$ to gain or variation of TS AC output voltage $V_{OUT_{TS}Lock-in}$ to gain. They are detailed in Section 5.3
- *Homodyne*: A homodyne measurement introduces one single input signal of known characteristics (frequency, modulus and/or phase) and is compared to other measurements in the circuit. The theory on homodyne temperature measurements is found in Section

3.3.3 and the homodyne signatures are in Section 5.3.1

- *Heterodyne*: *homodyne* measurement introduces two input signals of known characteristics (frequency, modulus and/or phase) with a small frequency difference between each other Δf_s. The theory on homodyne temperature measurements is found in Section 3.3.4 and the homodyne signatures are in Section 5.3.2

- $N\,(TS)$: DAC integer value that controls the current mirror biasing the temperature sensors TS 1 and TS 2

- *Lock-in amplifier*: A lock-in amplifier is a type of amplifier that can extract a signal with a known carrier wave from an extremely noisy environment

3 Theory Frame

3.1 Direct and indirect measurements

Performing a direct electrical measurement on a circuit modifies its behavior intrinsically, as the sensor modifies the electrical topology by adding elements and electric charges are added to the circuit nodes being measured. A direct measurement example is measuring voltages and currents to calculate output and/or input power, to get gain.

Indirect measurements, on the other hand, quantify a different magnitude that is known to have a relation to the wanted magnitude. Indirect measurements have a much smaller effect on the system (a circuit in the electrical case at hand) by comparison to direct measurements, being much less intrusive and sometimes simpler in their practical nature. An example of indirect measurements is weighing water by measuring its volume.

3.2 Need of gain signatures

The present effort to monitor the gain in RF PAs using temperature measurements requires linking particular absolute or difference temperature measurements to values or changes in the PA gain.

The gain and temperature are related in the PAs, but not in a straightforward way. There is a strong dependence on thermal coupling, sensitivity and other effects.

The real-world implementations measurable in the laboratory require the study of experimental relations between the temperature measurements and the PA gain. These temperature-gain signatures will have specific, repeatable shapes but present different values for the different ICs measured, accounting for the statistic process variability in manufacturing.

The gain signatures will characterize the temperature-gain relation for each chip with their specific values, a sort of *individual thermal identifier of the gain*. The evolution of the signatures after Aging is applied, when having the previous signature stored, would allow recalibration to operate at the previous gain.

3.3 Temperature in RF power amplifiers

3.3.1 Temperature sensor

The usage of a differential temperature sensor TS as an indirect measurement of gain (an electric magnitude) is proposed by [1]. A differential temperature sensor measures a difference of temperatures between two sensor terminations placed in different areas of the IC, having much better common mode rejection CMR than its single-ended temperature sensor counterpart. The voltage output of a basic temperature sensor is shown in 1.

A single-ended implementation would require calibration and have high offset to be corrected, but a differential temperature sensor will measure the differences in thermal coupling between the end of the sensor on top of the PA and the other end in a far-away region in the IC.

$$V_{OUT_{TS}} = k(T_2 - T_1) \quad (1)$$

The implementation with a differential temperature sensor consists of one BJT transistor on the PA area in a different layer, not electrically connected to the PA, and the BJT at a further distance than thermal coupling by the PA can reach, consisting of the second end of the differential temperature sensor.

Electric power in the PA generates a temperature variation measurable by the temperature sensor with a voltage output. Since the TS has two sensing ends at a relatively close and far distance respectively, the temperatures T_2 and T_1 in 1 are defined by how much heat has been able to transfer to each area by thermal coupling.

$$P_{DC} \rightarrow \Delta T$$

3.3.2 Thermal coupling

The *Joule effect* is caused by free carriers impacting with impurities, phonons and themselves in a conducting material in which a voltage difference is applied, generating heat and increasing temperature.

$$P = V \cdot I \tag{2}$$

The heat generated by the Joule effect can be expressed as power, as shown in Eq. 2. In stationary state the heat transfer is an energy flux between the heat source and drain. This phenomenon follows inside the IC Fourier's Law of Heat Transfer in solid materials. Thermal coupling is the relation between the dissipated power in a specific point location in the IC (the PA in the application at hand) and the temperature reached in another region of the IC.

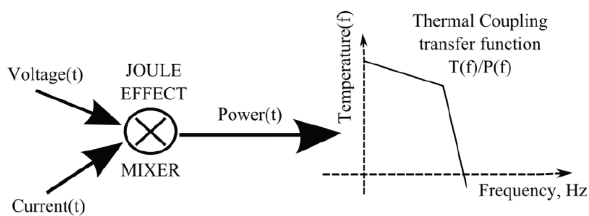

Figure 1: Circuital model of the thermal coupling mechanism, extracted from Figure 2 in [2].

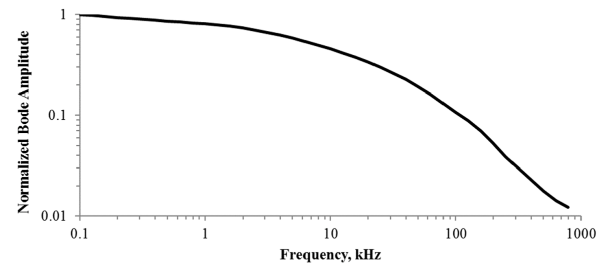

Figure 2: Example of thermal coupling. Normalized frequency response. CUT is a MOS transistor (dimensions: W = 100 μm, L = 10 μm) at a 25 μm distance from the temperature transducer. Extracted from [3].

Thermal coupling in the IC substrate behaves as a low pass filter LPF with distance. Frequencies higher than 100kHz do not travel further than tens of nm, which means that AC and RF temperature components normally are contained nearby the region they are produced on. However, if an unwanted source of thermal coupling is too near an area of interest (such as a power amplifier or a temperature sensor), this thermal coupling will be added to the total measured by the sensor. Figure 2 shows the thermal coupling frequency response measured in [3]. The gain for

the base input RF frequency f_s used later in this thesis is greatly attenuated at small distances in the IC. This means that the RF component of the heat at $f_s = 100MHz$ will not transfer along the IC to the further differential sensor node.

3.3.2.1 Power dissipated by the input resistor R_{bias} The resistor between the current mirror that biases the gate DC level $V_{GS_{DC}}$ and the decoupled RF input signal v_{IN} in the PA gate dissipates a small amount of power in DC. In Eq. 3, in the fraction resulting of the power of 2 of the sinusoidal signal, the $\frac{1}{2}$ term represents DC voltage while the term $\frac{cos(2\omega t)}{2}$ represents AC voltage.

$$
\begin{aligned}
v_R^2 = (V_R \cdot cos(\omega t))^2 = V_R^2(\frac{1 + cos(2\omega t)}{2}) \\
P_R = \frac{V_R^2}{2R} \leftarrow V_R = V_{GS} - V_{IN}; R = 1.655k\Omega
\end{aligned}
\tag{3}
$$

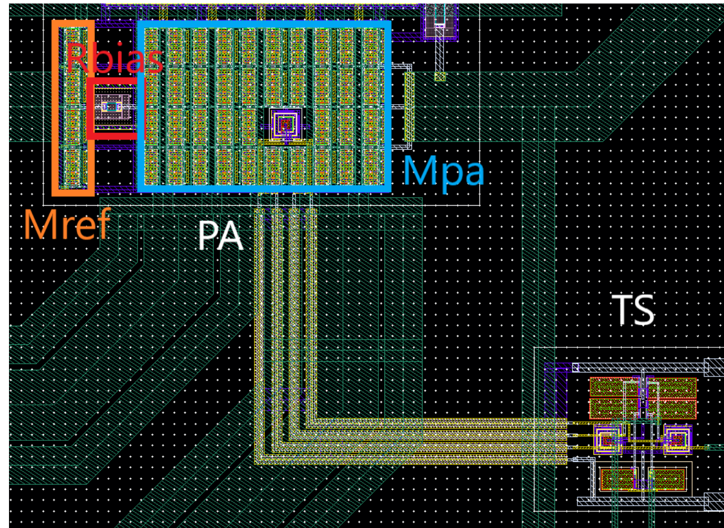

Figure 3: Layout of a PA and its TS in the IC PAAGEANT. Orange marks the reference transistor at the PA biasing, red marks the R_{bias} separating the DC biasing and RF input and blue marks the PA transistor.

3.3.2.2 Power dissipated subfolding The total DC dissipated power has two components in an RF power amplifier that may be named *subfoldings*. The first dissipated power subfolding [0]x[0] is caused by the DC drain current and DC source voltage $I_{D_{DC}} \cdot V_{DD}$ when biasing the PA, and increases with P_{IN}. The second dissipated power subfolding [1]x[1] is the DC resulting power decrease from applying an RF signal, being negative decreases the total dissipated power when P_{IN} increases. With large RF signal power, the biasing point in the PA changes and gain is further lost.

3.3.3 Homodyne temperature measurements

A *homodyne* measurement introduces one single input signal of known characteristics (frequency, modulus and/or phase) and is compared to other measurements in the circuit.

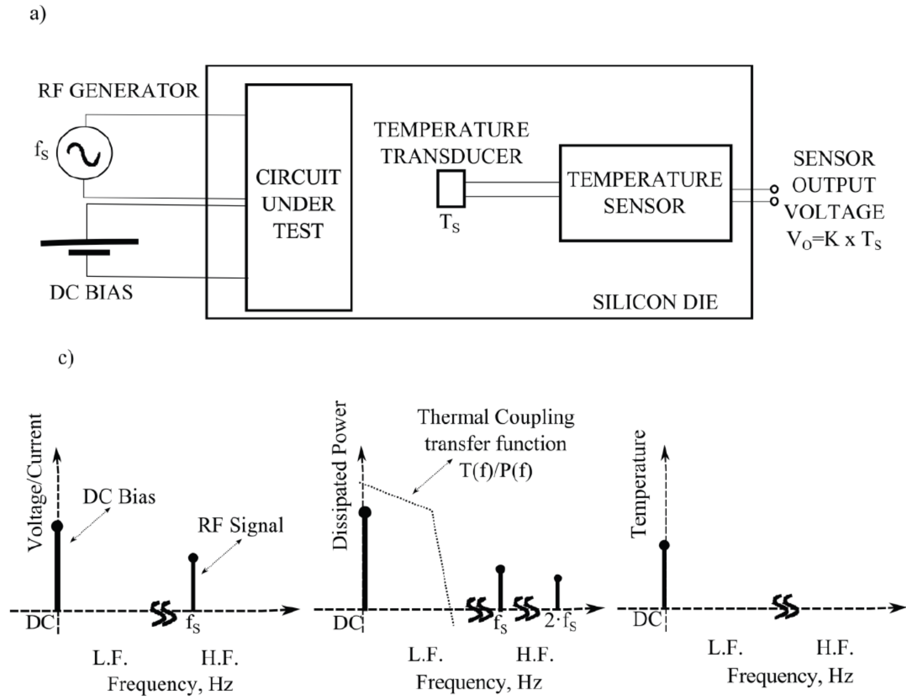

Figure 4: Description of the physical mechanisms that take place in built-in homodyne temperature measurements: a) a linear CUT and a temperature sensor are placed in the same silicon die, c) spectral components of the CUT electrical signals, power dissipated by the CUT and temperature at the transducer location with homodyne excitation. Extracted from Figure 2 in [2].

In the application at hand, the PA is biased in DC and a single RF signal is introduced at the input with frequency f_s and power P_{IN}. The voltage in the PA is Eq. 4 and the current is Eq. 5.

$$v(t) = V_{DC} + A \cdot cos(2\pi f_s t) \tag{4}$$

$$i(t) = I_{DC} + B \cdot cos(2\pi f_s t) \tag{5}$$

The power dissipated in the PA in homodyne temperature measurements in low and high frequency are expressed in Eq. 6.

$$P(t) = [V_{DC}I_{DC} + \frac{AB}{2}] + [BV_{DC} + AI_{DC}]cos(2\pi f_s t) + \frac{AB}{2}cos(4\pi f_s t) \tag{6}$$

In cases where $f_s >> 100kHz$ (as in our application, using $f_s = 170MHz$), the high frequency (RF) component of the dissipated power in Eq. 6 is out of the transfer function of the LPF filter behavior of the thermal coupling. Therefore, only the DC component of the dissipated power increases the temperature around the PA and is measured by the nearby BJT end of the temperature sensor, described in Eq. 7.

$$T(t) = T_{DC} = R_{th} \cdot [V_{DC} I_{DC} + \frac{AB}{2}] = R_{th} \cdot P_{DC} \tag{7}$$

where R_{th} is the thermal coupling resistance between the PA and the sensor transducer and P_{DC} is the DC component of the dissipated power in homodyne. Note that the measured temperature depends on the DC bias values V_{DC} and I_{DC} and modulus of RF voltage A and current B, and has no dependence on the RF frequency f_s. The DC bias component of the temperature is a big part of the measured temperature, and it can be difficult to extrapolate the gain from the measurements.

3.3.4 Heterodyne temperature measurements

A *homodyne* measurement introduces two input signals of known characteristics (frequency, modulus and/or phase) with a small frequency difference between each other Δf_s. Their intermodulation produces many harmonics, but also a low frequency intermodulation product. This can be exploited with an LPF to make a measurement easier to implement. Also, the measurement is in a low frequency AC, separated from the DC value, so the noise and variation introduced by the DC bias are not so prevalent.

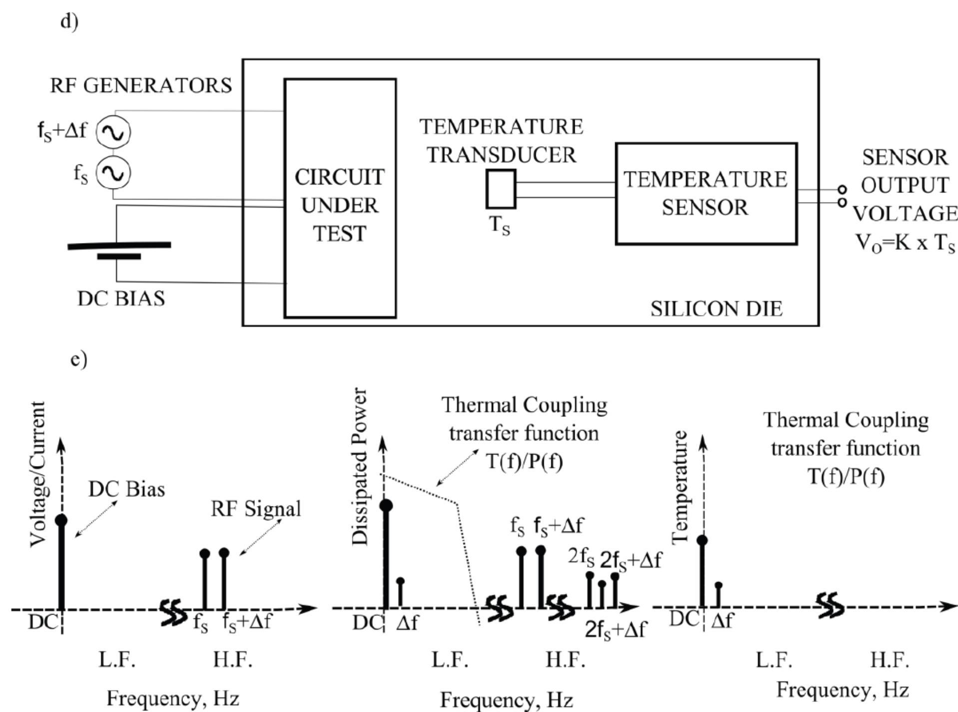

Figure 5: Description of the physical mechanisms that take place in built-in heterodyne temperature measurements: d) heterodyne CUT excitation, and e) spectral components under heterodyne CUT excitation. Extracted from Figure 2 in [2].

In the application at hand, the PA is biased in DC and a two RF signals at $f_{s_1} = f_s$ and $f_{s_2} = f_s + \Delta f$ are introduced at the input with frequency f_s and power P_{IN}. The voltage in the PA is Eq. 8 and the current is Eq. 9.

$$v(t) = V_{DC} + A \cdot [cos(2\pi f_s t) + cos(2\pi(f_s + \Delta f)t)] \tag{8}$$

$$i(t) = I_{DC} + B \cdot [cos(2\pi f_s t) + cos(2\pi(f_s + \Delta f)t)] \tag{9}$$

The power dissipated in the PA in heterodyne generates several spectral components, the two most interesting of which are expressed in Eq. 10.

$$P(t) = [V_{DC}I_{DC} + AB] + ABcos(2\pi f_s t) + higher\ frequency\ terms \tag{10}$$

Such lower frequency components of the dissipated power in Eq. 10 result in a measurable temperature change $T_{\Delta f}(t)$, described in Eq. 11, that can be measured by the nearby BJT temperature sensor transducer.

$$\begin{aligned} T(t) = R_{th} \cdot [V_{DC}I_{DC} + AB] + Z_{TH}(\Delta f) \cdot AB \cdot cos(2\pi\Delta f t) = \\ = R_{TH} \cdot P_{DC} + Z_{TH}(\Delta f) \cdot P_{\Delta f}(t) = R_{th} \cdot P_{DC} = T_{DC} + T_{\Delta f}(t) \end{aligned} \tag{11}$$

where $P_{\Delta f}(t)$ is the spectral component of the dissipated power at Δf and $Z_{TH}(\Delta f)$ is the thermal coupling impedance between the PA and the BJT transducer of the temperature sensor at frequency Δf, that is usually a complex value with real and imaginary components.

The DC temperature increase T_{DC} in Eq. 11 depends on the DC bias and the RF signal magnitudes AB. The temperature AC component $T_{\Delta f}(t)$ depends on the RF power (A and B), appearing in low frequency due to the downmixing and is independent of the frequency f_s. This AC component of the temperature $T_{\Delta f}(t)$ reaches the BJT transducer of the temperature sensor and is named lock-in temperature measurement, due to a lock-in instrument being used to measure it.

The heterodyne temperature measurement requires more and more complex instruments to be performed, but is advantageous to the homodyne measurement. The AC component temperature change (heterodyne, measured by the lock-in) only depends on the RF characteristics of the PA and not its DC bias, allowing a better characterization of the PA. Also, the value of Δf is controllable, so the temperature measurements are independent of the IC configuration and simplifies the calibration process.

The PA operating point being set by $V_{GS_{DC}}$ does affect its gain and therefore the output power and the measured temperature, but the temperature measurement is not being affected by $V_{GS_{DC}}$, rather the output power and temperature change with $V_{GS_{DC}}$.

4 Implementation

4.1 PAAGEANT Chip

The PAAGEANT IC has been designed and manufactured to demonstrate the pre-aging characterization and post-aging recalibration to operate at the original gain using only temperature measurements using homodyne and heterodyne methods proposed by [1] and [2]. The PAAGEANT IC is part of the TOGETHER national project and has been previously simulated and tested in other projects.

The IC design consists of 3 power amplifiers PA with combinations of temperature sensors TS and power sensors PS, detailed in Section 4.1.2, using the CMOS 350nm AMS technology. This project uses the PAAGEANT IC to characterize PA 1 and TS 1 and propose temperature-gain signatures. 11 ICs were measured in the laboratory, their results presented in Section 5.

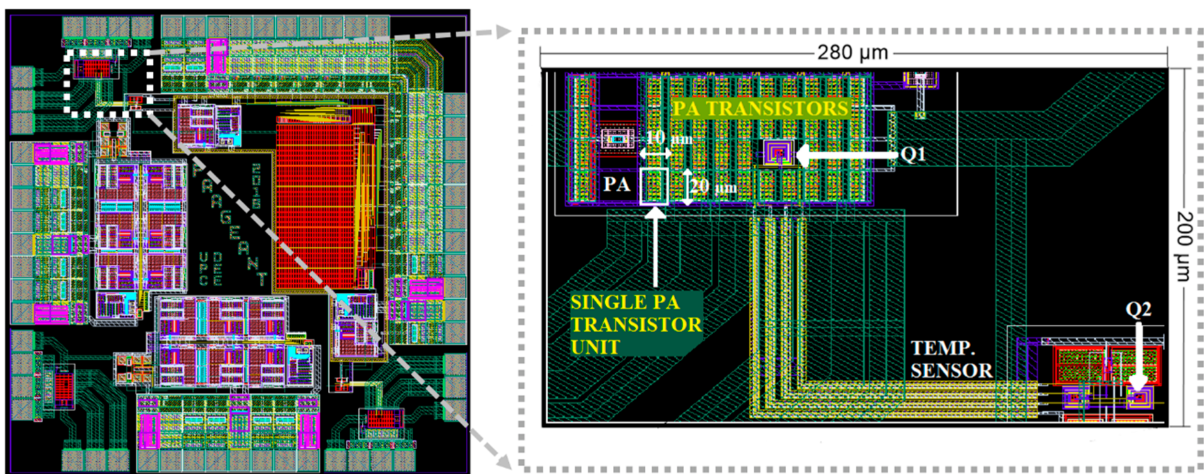

Figure 6: Layout of the PAAGEANT IC.

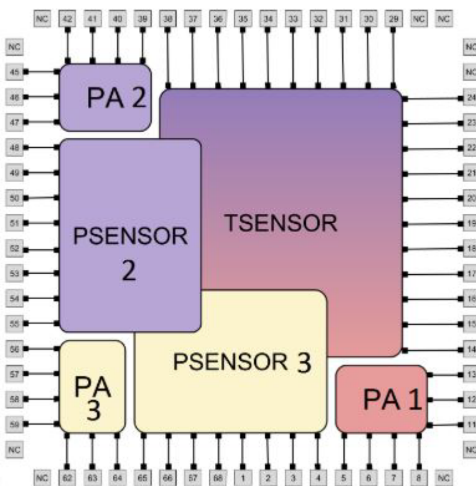

Figure 7: PAAGEANT IC block layout, extracted from [4].

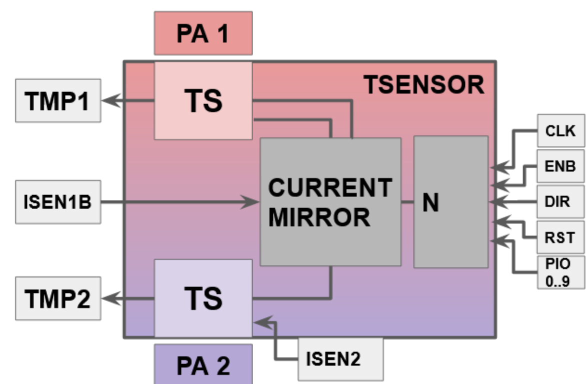

Figure 8: Temperature sensor biasing structure (simplified) of the PAAGEANT IC.

4.1.1 Differential temperature sensors in PAAGEANT

DC power in the circuit generates a temperature variation measurable by the temperature sensor with a voltage output. A simple differential temperature sensor output has a very high sensitivity, but the dynamic range in temperature is very small, as seen in Figure 9.

The saturation region at the top and bottom voltage values can be seen, and the desired linear region has high sensitivity but very small dynamic range in temperature. The temperature sensors in the PAAGEANT IC have a biasing circuit that can shift the voltage-temperature curve, showing the extended dynamic range in Figure 10.

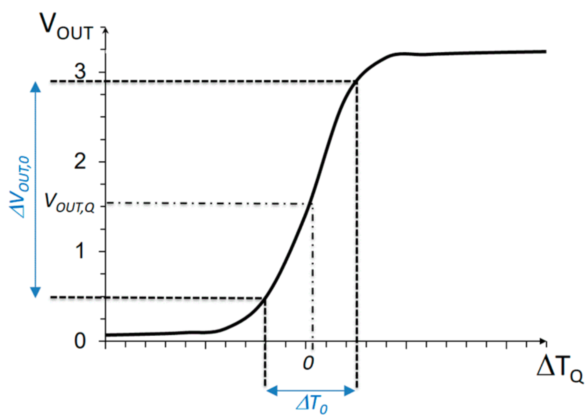

Figure 9: Typical characteristic curve of the core temperature sensor. Extracted from Figure 4 in [1].

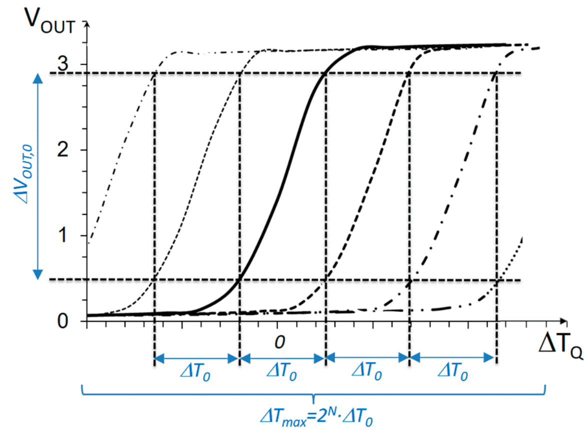

Figure 10: Characteristic curve of the differential temperature sensor with an extended dynamic range. Extracted from Figure 5 in [1].

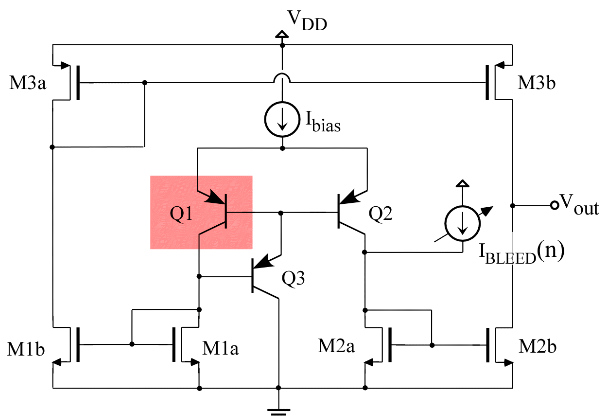

Figure 11: Schematic of the core circuit of the temperature sensor with current bleeding for extended dynamic range and variability compensation. Transistor Q1 is placed by the CUT and away from Q2 and the rest of the sensor. Extracted from Figure 6 in [1].

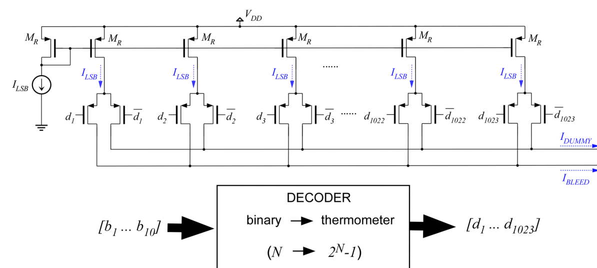

Figure 12: Scheme of the 10-bit current-steering DAC designed for the implementation of the bleeding current $I_{BLEED}(n)$, based on unary-weighted current sources. Extracted from Figure 13 in [1].

This is achieved with the TS circuit in Figure 11. The current mirror $I_{BLEED}(n)$ in Figure **??** is controlled by a 10-bit DAC, thereby shifting the voltage-temperature curve and extending

the measurable temperature range. With the DAC output N we shift the operating point to be measuring voltage where it is most sensitive. Therefore, the DAC output N is an indirect temperature measurement.

$$P_{DC} \rightarrow \Delta T \rightarrow \Delta V(\Delta N)$$

Searching for the central N where $V_{OUT_{TS}} = \frac{V_{DD}}{2}$ by increasing its value by 1 can slow down the experimental programs, which is very inconvenient in the laboratory. To speed up measurements, a binary search algorithm has been implemented that in 14 searches (about 10 seconds) finds the desired N value.

4.1.2 Different sensor configurations in PAs

Figure 8 shows the different biasing strategies used in TS 1 (PA 1) and TS 2 (PA 2). A current mirror is controlled by the DAC N from the Arduino digital inputs and biasing input I_{SEN1b} (as voltage V_{SEN1b}) and second biasing I_{SEN2} for TS 2 and a current copy of ratio 1:1792 for TS 1. Table 1 details the power amplifier - sensor configurations.

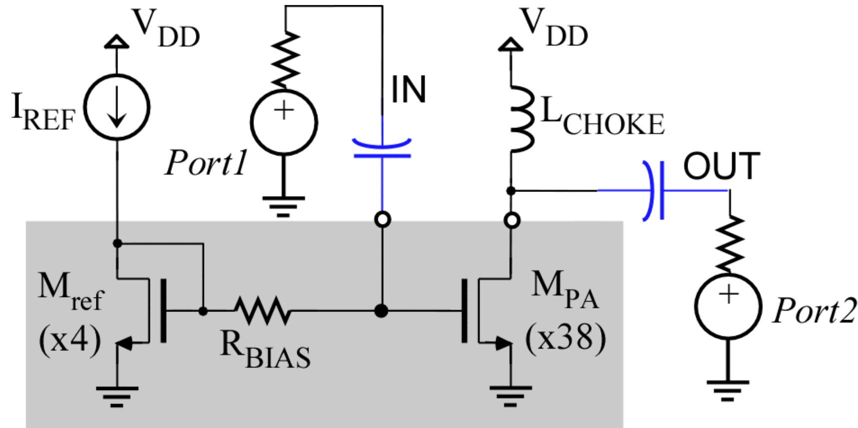

Figure 13: PA schematic in the PAAGEANT IC.

Configuration	PA 1	PA 2	PA 3
Power Sensor	None	PS 1	PS 2
Temperature Sensor	TS 1	TS 2	None
TS biasing	internal copy	external instrument	N/A
TS biasing method	V_{SEN1b}	V_{SEN1b} and I_{SEN2}	N/A

Table 1: Sensor configurations of the different PAs in the PAAGEANT IC.

4.1.2.1 PA 1 The PA 1 includes TS 1 and no internal PS. The current biasing of the current mirror branch in TS1 is done via an internal copy of ratio 1:1792, so only the bias voltage V_{SEN1b} must be set externally in a range of $2.3V \leq V_{SEN1b} \leq 2.5V$.

4.1.2.2 PA 2 The PA 2 includes TS 2 and internal PS. The TS 2 is biased with two degrees of freedom: bias voltage V_{SEN1b} and current I_{SEN2}. I_{SEN2} can also be biased with a voltage

source, calling it V_{BLEED}.

4.1.2.3 PA 3 Not including a temperature sensor, the PA 3 in the manufactured chips cannot be directly used for the purposes of this study. However, in the further study of using temperature sensors and signatures to calibrate for equal gain after Aging, this PA is useful to study the changes Aging introduces to the characteristics of the PA.

This PA can be characterized with the internal PS and external power sensors and studied as Aging is applied to the PA. The changes in the PA characteristics can be used to predict the changes in PA 1 and PA2 that have a temperature sensor TS and choose the best parameters and strategies to study them before and after the Aging process.

4.2 Instruments used in the measurements

The instruments in Table [2] are used to power, bias and measure the PAAGEANT IC and PCB. They are connected to a laboratory computer running MATLAB code and communicate via the GPIB and the LAN (TCPIP0) interfaces.

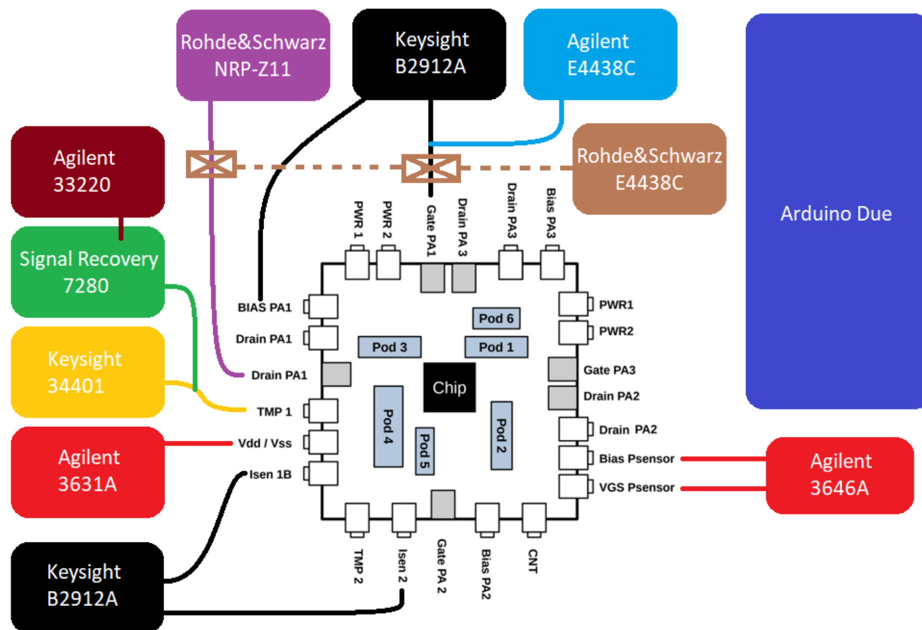

Figure 14: Connections diagram of the PCB and instrumentation.

4.3 Code

In order to make laboratory measurement time as efficient as possible, the MATLAB code has been structured separating measurements from post-processing and plotting. Characterization can be done by sweeping biasing and input RF variables in a chosen set of parameters, and their graphical representation and study is a process that can be done entirely separated.

To this end, the MATLAB code created for this study automates the configuring of the tests and programs, automatically organizes the results in subfolders and saves all experiment data (parameters and measurements) in the respective subfolders. The post-processing code is run after each experiment to generate plots and allow critical study on-site, but much emphasis has

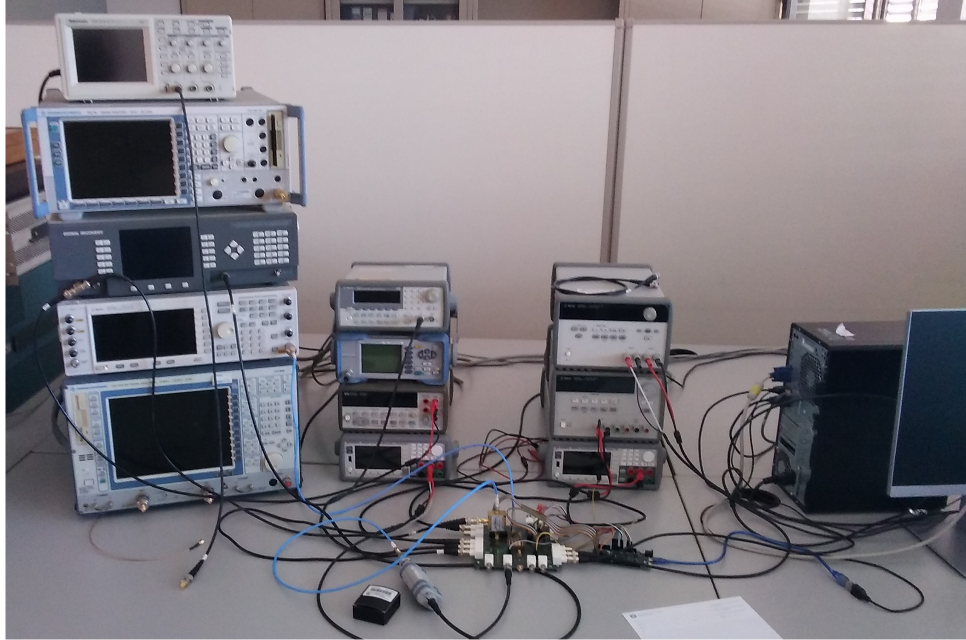

Figure 15: Laboratory setup.

Usage	Type	Brand	Model
V_{DD} bias	DC source	Agilent	E3631A
PS bias	DC source	Agilent	E3646A
PA bias: V_{DS}, V_{GS}	DC source	Keysight	B2912A
TS bias: V_{SEN1b}, I_{SEN2}	DC source	Keysight	B2902A
Input RF signal	RF source	Agilent	E4438C
$V_{out_{TS}}$	DC measurement	Keysight	34401A
$N, V_{out_{TS}}, ambient\ temp, V_{out_{PS}}$	Digital I/O, ADC and DAC	Arduino	Due
P_{OUT}	Power measurement	Rohde & Schwarz	NRP-Z11
Reference signal to Lock-in	AC square signal source	Agilent	33220A
Heterodyne $V_{OUT_{TS}}$	Lock-in	Signal Recovery	7280
S Parameters	Vector Network Analyzer	Rohde & Schwarz	E4438C

Table 2: Instruments used to bias and measure the PAAGEANT IC.

been put so that changes and improvements in the post-processing and plots made afterwards are automatically applied to all measurements done previously.

Each experiment program performs a set of measurements to obtain a particular characteristic or group of characteristics, by sweeping a group of variables. In their naming, X is 0 (no PS bias) or 1 (with PS bias) and Y the particular experiment programs. If not stated otherwise, the programs use $V_{DS} = 3.3V$, $V_{GS} = 0.89V$, $V_{SEN1b} = 2.5V$, $f_s = 170MHzV$ and $\Delta f = 10013Hz$ when applicable.

[Total duration $\approx$ 3h] [Total duration repeating with PS $\approx$ 6h]

4.3.1 A0*Y*: DC and RF characterization of the PA

[Total duration $\leq$ 10min] Power Amplifier characterization.

4.3.1.1 A03: AC frequency response [Duration = 1min 50s] Sweep $f_s = [25 : 25 : 700]MHz$ and $V_{GS} = [0.74 : 0.5 : 1.04]V$ to observe how the gain and drain current $I_{D_{DC}}$ change with frequency for different V_{GS} biasing.

4.3.1.2 A04: 1dB compression point with f_s. [Duration = 0min 55s] Sweep $P_{IN} = [-20 : 1 : 10]D$ and $f_s = [100, 170, 200]MHz$ to find the 1dB compression points for each f_s.

4.3.1.3 A05: RF gain characteristics [Duration = 5min 20s] Sweep $P_{IN} = [-20 : 1 : 10]D$ and $V_{GS} = [0.74 : 0.2 : 1.04]V$

4.3.1.4 A06: I_D characterization to V_{GS} and V_{DS} [Duration = 2min 30s] Sweep V_{DS} and V_{GS} for $P_{IN} = OFF$. Helps find the V_T and see the drain current $I_{D_{DC}}$ curves.

4.3.2 B*XY*: Homodyne, TS sensor and thermal coupling characterization and gain signatures

[Total duration $\leq$ 1h 45min]

4.3.2.1 BX1: TS non-bias voltage-temperature curve [Duration = 4min] Sweep TS DAC (N) and measures $V_{OUT_{TS}}$ for different sensor bias V_{SEN1b} while $V_{DS} = 0V$ and $V_{GS} = 0V$.
Sensitivity and Dynamic Range for non-biased.

4.3.2.2 BX2: TS bias voltage-temperature curve and TS sensitivity and dynamic range. [Duration = 5min 45s] Sweep TS DAC (N) and measures $V_{OUT_{TS}}$ for different sensor bias V_{SEN1b} while $V_{DS} = 3.3V$ and $V_{GS} = 0.89V$.
Sensitivity and Dynamic Range for biased.

4.3.2.3 BX3: TS voltage-temperature curve for non-bias, bias and bias with input RF signal [Duration = 5min] Sweep TS DAC (N) and measures $V_{OUT_{TS}}$ for sensor bias $V_{SEN1b} = 2.5V$. Bias with input uses $V_{DS} = 3.3V$, $V_{GS} = 0.89V$ and $P_{IN} = 0dBm$. Visual representation of biasing and RF input to the thermal coupling.

4.3.2.4 BX5: Signature 2 (2a and 2b) [Duration = 50min] Sweep P_{IN} and V_{GS}, find the best TS DAC (N) in each measure.
Signature 2a: $Gain(\Delta N)$; $N@P_{IN} = [-5, 5]dBm$ for each V_{GS}.
Signature 2b: $Gain(\Delta N)$ and $I_D(\Delta N)$; $N@P_{IN} = [OFF, -20]dBm$ for each V_{GS}.

4.3.2.5 BX6: Thermal coupling from biasing [Duration = 2min] Sweep V_{DS} and V_{GS}.
DC thermal coupling due to the bias point.

4.3.2.6 BX7: Thermal coupling from $P_{R_{IN}}$ [Duration = 1min] Non-bias with RF input $P_{IN} = -10dBm$.
DC thermal coupling due to the input resistor R_{bias}.

4.3.2.7 BX8: Signature 1 [Duration = 30min] Sweep P_{IN} and V_{GS}, use a static TS DAC (N) chosen best for each V_{GS} and measure $V_{OUT_{TS}}$.
Signature 1: $Gain(\Delta V_{OUT_{DC}}); V_{OUT_{TS}}@P_{IN} = [-20, -10]dBm$ for each V_{GS}.

4.3.3 C*XY*: Heterodyne temperature characterization and gain signatures

4.3.3.1 CX4: Signatures 3 and 4 [Duration = 1h] Sweep P_{IN} and V_{GS} with $\Delta f = 10013MHz$.
Signature 3: $Gain(slope\ log(V_{OUT_{TS} Lock-in}) - kP_{IN})$ for each V_{GS}.
Signature 4: $P_{OUT}(slope\ log(V_{OUT_{TS} Lock-in}) - kP_{IN},);\ N@P_{IN} = [OFF, -20dBm]$ for each V_{GS}.

4.3.4 D*X*1: S Parameters characterization

[Duration = 0min 30s] Switch on the Relay to connect the PA input and output to the VNA that computes the S parameters.

4.3.5 E01: Convert data

[Duration = 1min/experiment set] Allows deleting and/or regenerate all figures or a selection of them from the $.mat$ files containing all the experiments results.

4.3.6 E02: Plot figures

[Duration = 10s/experiment] Computes relevant post-processing characteristics such as sensitivity or dynamic range and plots all figures respective to the current experiment running.

4.3.7 E03: Post-process all ICs signatures and characteristics

[Duration = 10s] Performs the statistical analysis and plots of all the important TS characteristics and signatures.

5 Measurements

5.1 Power Amplifier characterization

The automated testing thoroughly characterizes each PA as well as its TS. Doing so allows comparing temperature data and thermal coupling among different ICs measured according to the actual electrical gain and drain current in their PAs.

The DC characterization of the PA MOS transistor is computed by Program A06: I_D characterization to V_{GS} and V_{DS} and shown in Figures 16 and 17. It will be of use to know the characteristics before and after applying Aging.

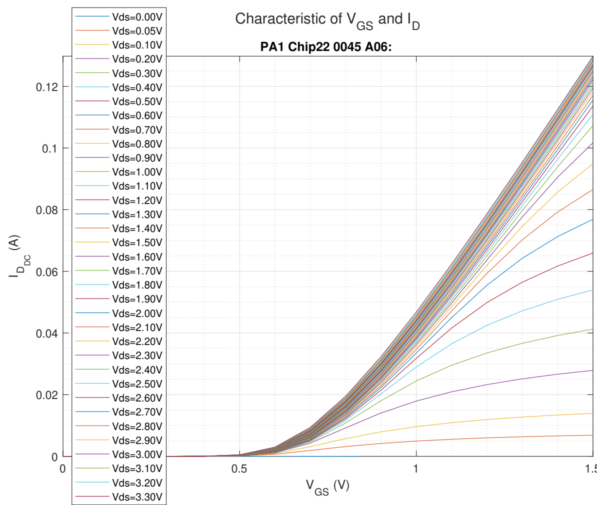

Figure 16: Drain current $I_{D_{DC}}$ characteristics vs V_{GS} of PA 1. $V_T = 0.05V$ is observed.

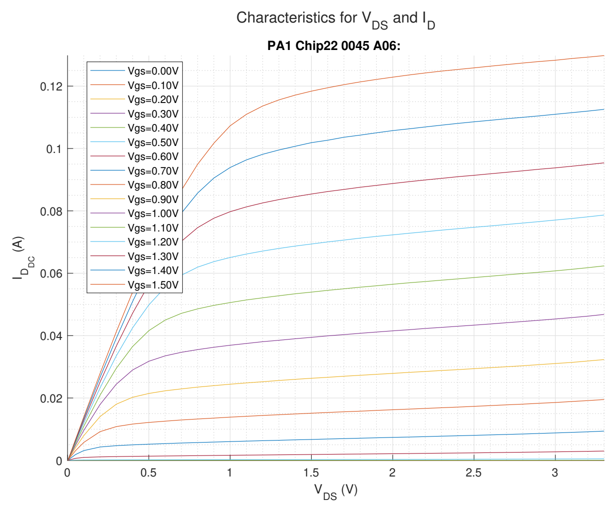

Figure 17: Drain current $I_{D_{DC}}$ characteristics vs V_{DS} of PA 1.

The DC operating point, with nominal PA bias of $V_{DS} = 3.3V$ and $V_{GS} = 0.89V$, is given by design. However, the ideal operating frequency f_s may have shifted in between design, simulation and manufacturing the ICs and their interaction in the PCB designed and manufactured to power, bias and measure the chips. To better characterize the PA in RF and study its gain, the best experimental frequency f_s must be chosen.

To do so, a sweep of f_s must be measured to see the gain in function of the frequency and biasing V_{GS}, and Program A03: AC frequency response accomplishes this goal. Figures 18 and 19 show the gain and drain current $I_{D_{DC}}$ vs base frequency f_s for several gate-source voltages V_{DS}. At around $f_s = 170MHz$ the nominal gain is 10.

Figure 20 shows the S Parameters measurements performed by Program DX1: S Parameters characterization. The input reflection coefficient S11 is at its lowest close to $f_s = 170MHz$ in all chips and similarly with output reflection coefficient S22, so this is frequency is chosen over the suggested $100MHz$ or $200MHz$. In Figure 21 the gain and current can be seen with the three frequencies, along with their 1dB compression points.

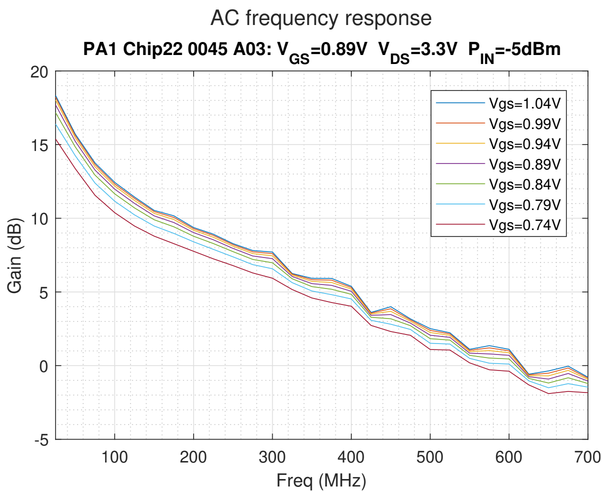

Figure 18: Gain characteristics for f_s of PA 1.

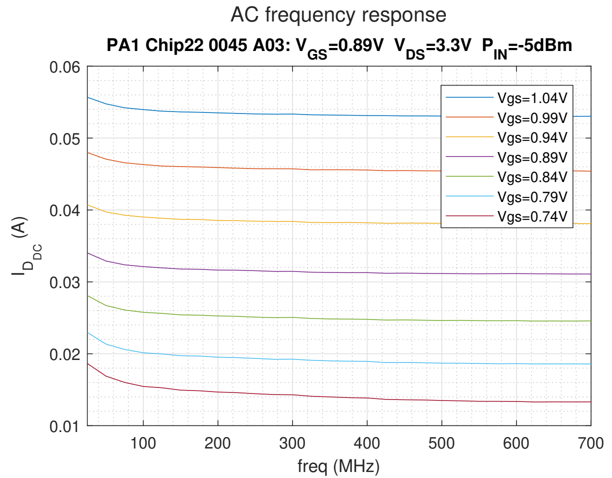

Figure 19: Drain current $I_{D_{DC}}$ characteristics for f_s of PA 1.

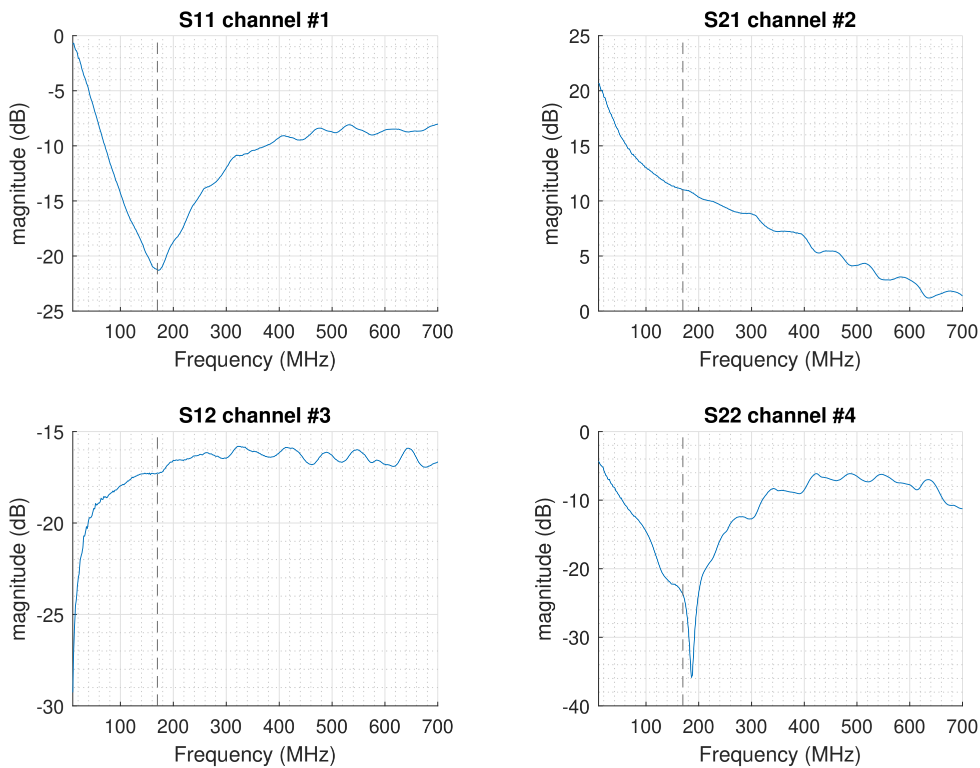

Figure 20: S parameters of PA 1.

The 1dB compression points for different frequencies f_s are computed by Program A04: 1dB compression point with f_s and depicted in Figure 21, while the 1dB compression points for different V_{GS} bias voltages are computed by Program A05: RF gain characteristics and depicted in Figure 22. The P_{IN} step value is $1dBm$, but it can be seen that for $P_{IN}0dBm$ for smaller V_{GS} bias voltages the gain is significantly affected and the 1dB compression points start appearing

at 6dBm, so 5dBm should be the maximum power used in signatures.

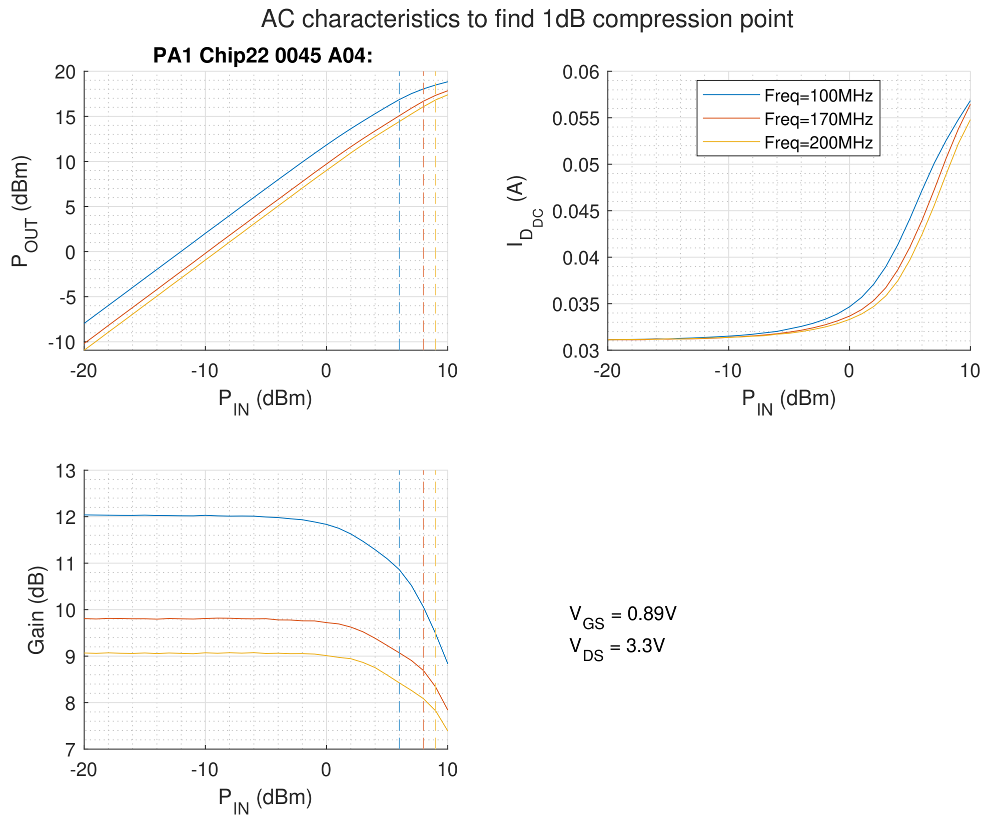

Figure 21: 1dB compression points of PA 1 around the operating frequency $f_s = 170MHz$.

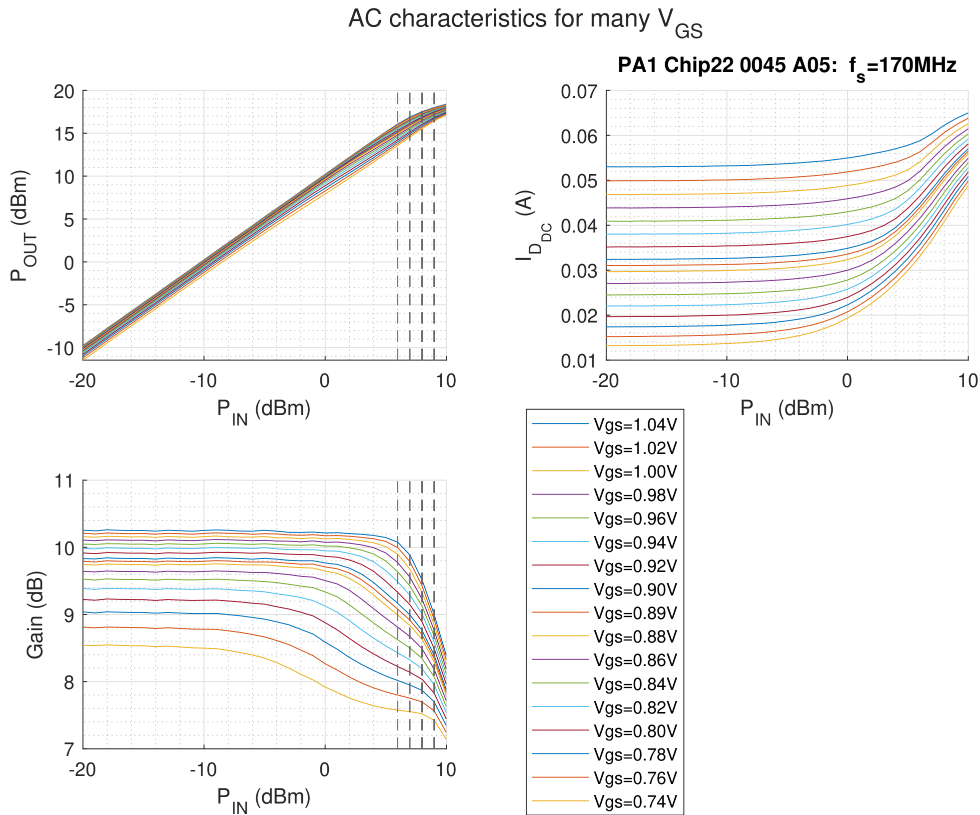

Figure 22: AC characteristics of PA 1 for different V_{GS}.

5.2 Quantifying thermal coupling

The design and behavior of the temperature sensors TS in the PAAGEANT IC is found in Section Differential temperature sensors in PAAGEANT. The following section will study its characteristics

5.2.1 Temperature Sensor characterization

The temperature sensors TS 1 and TS 2 operate by setting a DAC integer N to the current mirror so that the output voltage $V_{OUT_{TS}}$ curve central point is offset. The best value of N is set that has $V_{OUT_{TS}}$ at its central value ($\frac{V_{DD}}{2} = \frac{3.3V}{2} = 1.65V$), in the linear and very sensitive voltage region, and the value of N and $V_{OUT_{TS}}$ are stored.

As explained in section 4.1.2, TS 1 and TS 2 bias externally their current mirror in different ways, and their performance varies as a result. In the next measurements and characterizations, the TS 1 will be used and assumed, which sets the biasing of the current mirror with an internal copy of 1:1792 of the current that results from its bias voltage V_{SEN1b}.

The characteristics and performance of TS 1 depend on the bias voltage V_{SEN1b} applied. Therefore, the first step is choosing the most convenient V_{SEN1b}.

5.2.1.1 Sensitivity and Dynamic Range The different curves of the temperature measurement using TS 1 can be seen in Figure 23, where N sweeps and $V_{OUT_{TS}}$ measurements are performed with the PA non-biased (dashed lines) and biased (solid lines) for $V_{SEN1b} = [2.3, 2.4, 2.5]V$.

When biasing the PA, power is dissipated as heat and the thermal coupling is measured by the TS sensor as a shift in the voltage-temperature curve, so the central N has increased. The resulting sensitivity and dynamic range are displayed in Table 3.

The curve measurements to obtain the sensitivity and dynamic range are computed by BX1: TS non-bias voltage-temperature curve for non-biased and by BX2: TS bias voltage-temperature curve and TS sensitivity and dynamic range for biased.

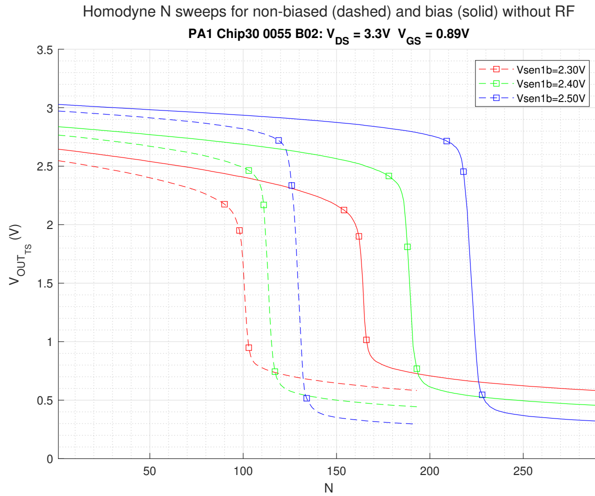

Figure 23: $V_{OUT_{TS}}$ vs TS DAC (N) sweep for different V_{SEN1b} bias voltages for the PA non-biased (dashed line) and biased (solid line) in Chip 30.

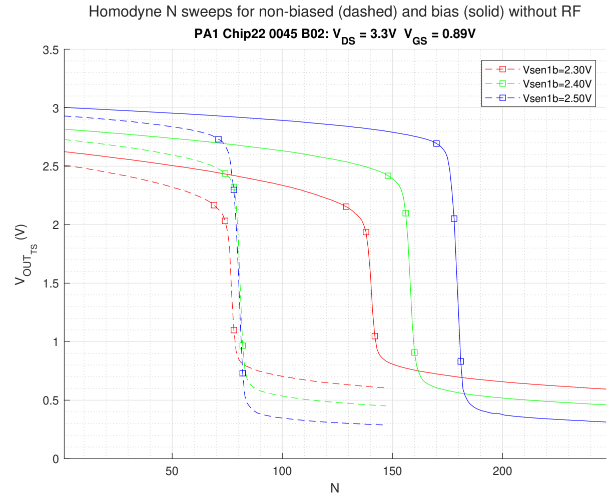

Figure 24: $V_{OUT_{TS}}$ vs TS DAC (N) sweep for different V_{SEN1b} bias voltages for the PA non-biased (dashed line) and biased (solid line) in Chip 22.

There are significant differences in the TS center N values for non-bias and bias between the different studied ICs, as seen when comparing Figures 23 and 24. Their drain currents I_D are also different, but not in such a significant degree. Also, some ICs have non-bias curves whose center N value decreases when increasing V_{SEN1b}. This difference in TS behaviors will affect the repeatability of the proposed signatures in Section 5.3. However, having the TS in each IC characterized allows for individual calibrations of the signatures to each particular IC.

The voltage curves shown in Figure 23 and the sensor characteristics shown in Table 3, particularly the superior Dynamic Range, show that $V_{SEN1b} = 2.5V$ is the best performing bias voltage for the current mirror of TS 1. Testing showed that with higher values the sensor did not operate properly and its sensitivity did not increase, so $V_{SEN1b} = 2.5V$ is the bias voltage chosen for TS 1.

The small variances shown in Table 3 when characterizing for the 11 chips indicate that the PAs in all ICs have different electrical characteristics and their TS reflect that in their measurements, but the TS characteristics are similar.

On one hand, Figures 25 and 26 show the non-biased and biases, respectively, sensitivity for the 11 measured ICs. On the other hand, Figures 27 and 28 show their dynamic range, non-biased and biased, respectively.

V_{SEN1b}	2.3 V	2.4 V	2.5 V
Sensitivity (non-bias) [V/#N]	0.33848	0.36007	0.35051
Variance σ^2	0.00313	0.00402	0.00402
Standard deviation σ	0.05592	0.06341	0.06339
Sensitivity (bias) [V/#N]	0.29677	0.32772	0.32630
Variance σ^2	0.00213	0.00221	0.00250
Standard deviation σ	0.04689	0.04696	0.04996
Sensitivity (bias) [#N/mW]			1.0004
Variance σ^2			0.01149
Standard deviation σ			0.10720
Sensitivity (bias) [V/mW]			0.32460
Variance σ^2			0.00246
Standard deviation σ			0.04961
Dynamic Range (non-bias) [V/#N]	1.2838	1.7463	2.2357
Variance σ^2	0.00116	0.00118	0.00150
Standard deviation σ	0.03410	0.03442	0.03879
Dynamic Range (bias) [V/#N]	1.2379	1.6895	2.2270
Variance σ^2	0.00181	0.00141	0.01902
Standard deviation σ	0.04260	0.03749	0.13790

Table 3: TS 1 (PA 1) characteristics for 11 chips measured. mW/N values only measured for chosen $V_{SEN1b} = 2.5V$ at section **??**.

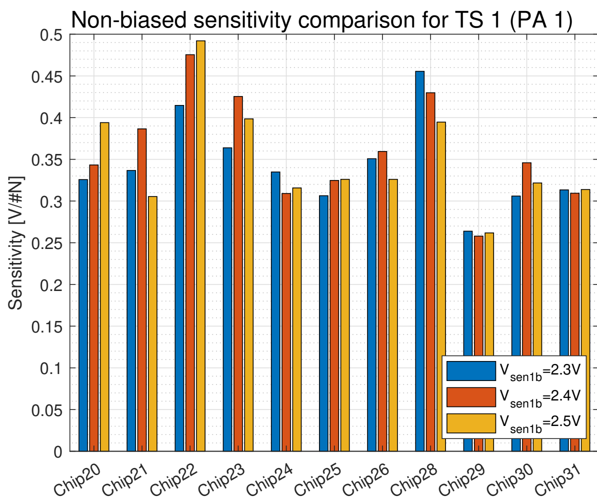

Figure 25: Non-biased sensitivity comparison for TS 1 (PA 1).

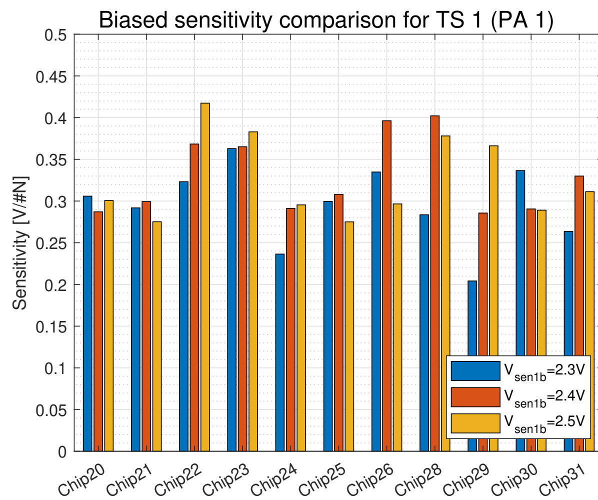

Figure 26: Biased sensitivity comparison for TS 1 (PA 1).

5.2.2 DC thermal coupling

The power dissipation causes an unbalance in the TS, so its measured voltage $V_{OUT_{TS}}$ goes to saturation region. The programs move the central N to have its TS output voltage at $V_{OUT_{TS}} = \frac{V_{DD}}{2}$.

Figure 3 shows in colored rectangles the main generators of heat, dissipating power that could

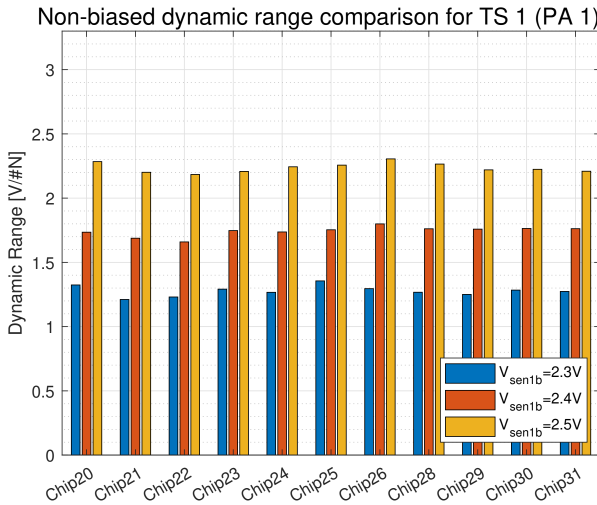

Figure 27: Non-biased dynamic range comparison for TS 1 (PA 1).

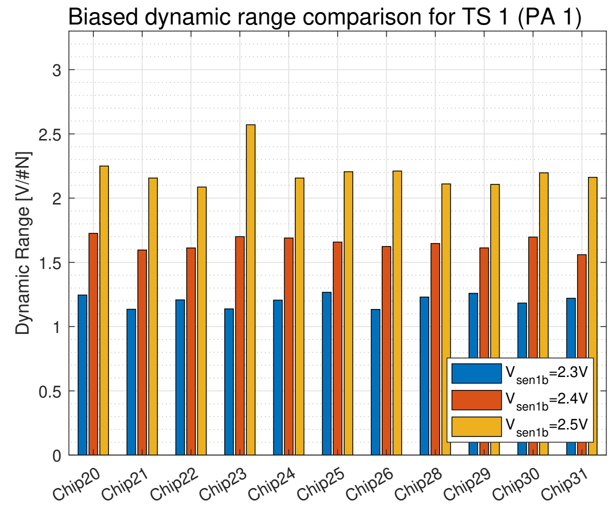

Figure 28: Biased dynamic range comparison for TS 1 (PA 1).

be measured by the TS by thermal coupling.

V_{SEN1b}	2.3 V	2.4 V	2.5 V
Thermal coupling P_{DC} [N]	67.5	81.8	105
Variance σ^2	26.1	42.4	104
Standard deviation σ	5.11	6.51	10.2
Thermal coupling P_{DC} [mW]			102
Variance σ^2			102
Standard deviation σ			10.0
Thermal coupling $P_{DC_{R_{IN}}}$ [N]	0	0	0
Variance σ^2	0	0	0
Standard deviation σ	0	0	0

Table 4: TS 1 (PA 1) thermal coupling for 11 chips measured.

5.2.2.1 DC thermal coupling due to the bias point Program BX6: Thermal coupling from biasing performs a V_{GS} and V_{DS} sweep without input RF signal to characterize the thermal coupling and the sensitivity in mW/N of the TS 1. The $V_SEN1b = 2.5V$ has already been chosen to get the best measurement, so it is the one used in program BX6.

On one hand, the results of the V_{GS} sweep for $V_{DS} = 0V$ in Figure 29 show that gate-source contribution to the bias thermal coupling is very small and not measured as an increase in the measured temperature N by the TS 1.

On the other hand, the results of the V_{GS} sweep for $V_{DS} = 3.3V$ in Figure 30 show a straight line of the dissipated power with the measured N of the TS 1. Therefore, the measurement of dissipated power (or temperature, as of Eq.7) with the DAC N of the TS 1 is a linear measurement. The slope and intercept of this measurement can be used for the sensitivity in mW/N and the thermal coupling as a bias offset value. The bias thermal coupling for the 11 ICs measured is detailed in Table 4 and the sensitivity in mW/N in Table 3.

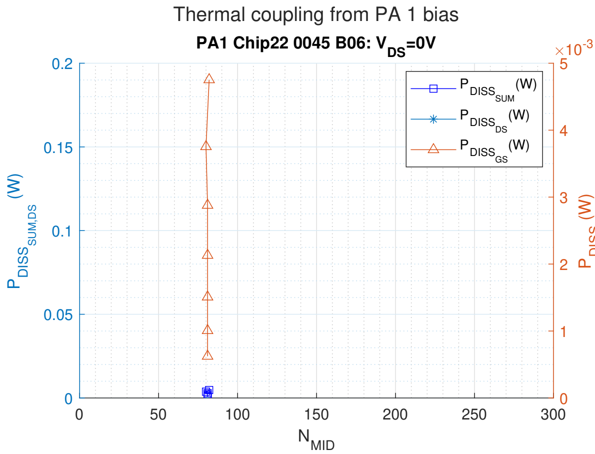

Figure 29: DC thermal coupling due to the gate-source bias point of PA 1. The different points correspond to values of $V_{GS} = [0.74, 0.79, 0.84, 0.89, 0.94, 0.99, 1.04]V$.

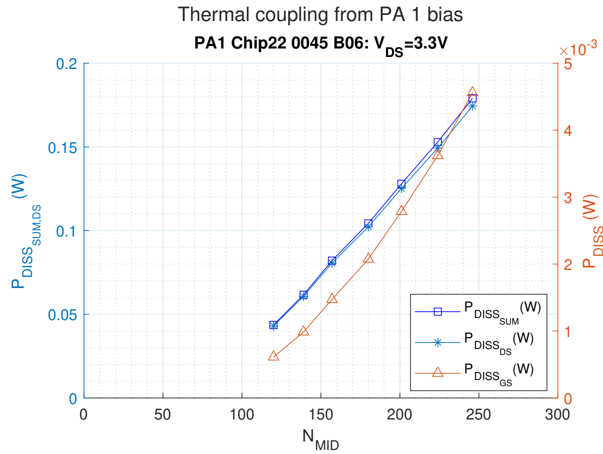

Figure 30: DC thermal coupling due to the drain-source bias point of PA 1. The different points correspond to values of $V_{GS} = [0.74, 0.79, 0.84, 0.89, 0.94, 0.99, 1.04]V$.

5.2.2.2 DC thermal coupling due to the input resistor R_{bias} The input resistor R_{bias} has a contribution to the DC thermal coupling as defined in Eq. 3. This is measured by Program BX7: Thermal coupling from $P_{R_{IN}}$ by having no other bias sources ($V_{GS} = 0V$ and $V_{DS} = 0V$) and applying an input RF signal $P_{IN} = -12dBm$. The thermal coupling contribution due to the input resistor is so small it is not measurable by the DAC N of the TS 1.

5.3 Gain signatures

4 gain signatures from temperature measurements have been proposed. They use homodyne and heterodyne methods and different measured variables to perform gain estimation.

The procedure to propose and study the signatures will be the following:

- Choose a type of measurement of temperature to relate to gain: $\Delta V_{OUT_{TS}}$
- Choose a range of P_{IN} values to use if the type of measurement of temperature requires it. Signature 1 does require this.
- compute the signature normalizing to the IC sensitivity and plot the Signature as a scatter plot
- perform a polynomial fitting that helps
- Post-process the signature to all measured ICs
- Compare and show the mean and variance of the polynomial fittings of the signatures of the 11 ICs.

5.3.1 Homodyne gain signatures

Signatures 1 and 2 use the two possible temperature measurements ($V_{OUT_{TS}}$ and the DAC central N that has $V_{OUT_{TS}} = 1.65V$) to obtain gain signatures.

5.3.1.1 Signature 1: $Gain(\Delta V_{OUT_{DC}}); V_{OUT_{TS}}@P_{IN} = [-20, -10]dBm$

BX8: Signature 1 uses the temperature sensor output voltage $V_{OUT_{TS}}$ for a fixed N that is chosen with RF input $P_{IN} = -20dBm$ for each V_{GS}. The choice of individual DAC N of TS 1 for each bias voltage V_{GS} at $P_{IN} = -20dBm$ and not one single is due to the high voltage-to-N sensitivity of the sensor. While two values could be close together enough to be in the linear voltage region shown in Figure 23, the rest of differently V_{GS} biased output voltages $V_{OUT_{TS}}$ would lie outside their dynamic range and not be accurate temperature measurements. Therefore, it is more accurate for Signature 1 to choose the most suitable N for each bias voltage V_{GS} and see its own evolution when increasing P_{IN}.

The effects of the DC power dissipation subfolding mentioned in Section 3.3.2.2 can be seen in the evolution of $V_{OUT_{TS}}$ for a fixed N in their different bias voltages V_{GS} in Signature 1, as seen in Figure 31. The power dissipation subfolding is visualized in the temperature sensor output voltages $V_{OUT_{TS}}$ decreasing with increasing P_{IN} for the higher values of V_{GS} and increasing with P_{IN} for the lower values of V_{GS}. Increasing the RF input power P_{IN} increases the temperature for the lowest V_{GS} and decreases the temperature for the higher V_{GS}.

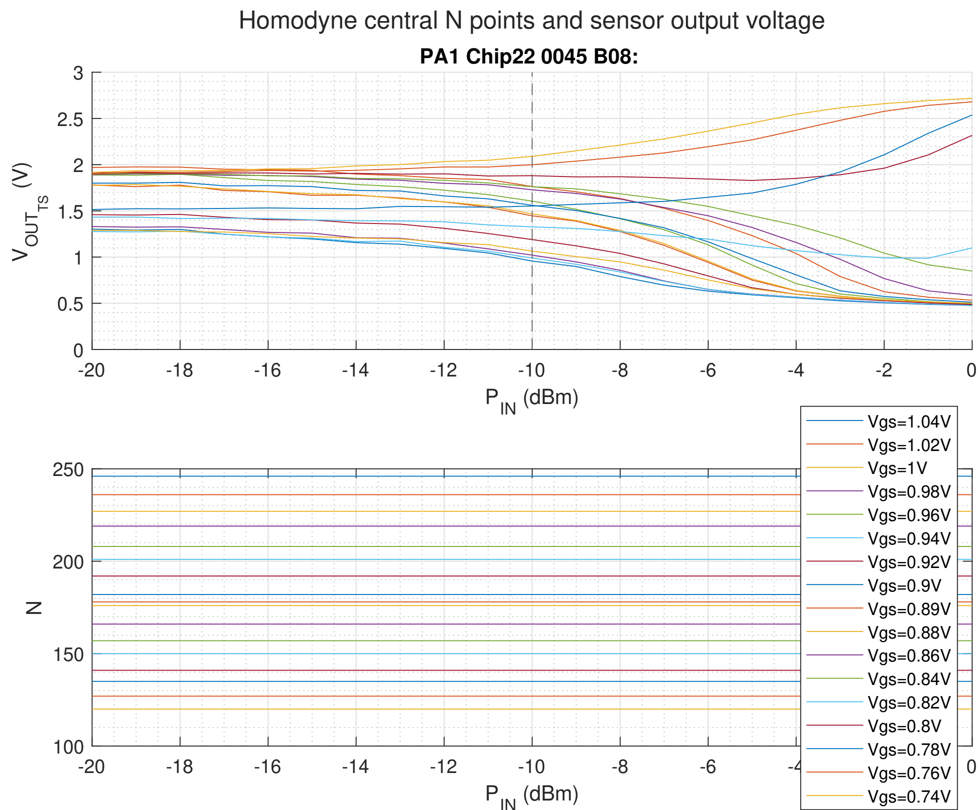

Figure 31: Temperature sensor output voltage $V_{OUT_{TS}}$ (top) for fixed N (bottom) used in Signature 1 of TS 1 (PA 1), measured at $P_{IN} = [-20, -10]dBm$ for chip 22.

The choice of right $P_{IN} = -10dBm$ to compare $V_{OUT_{TS}}$ to $P_{IN} = -20dBm$ is done experimentally. The $Gain(V_{GS})$ evolution is portrayed in Figure 22 to be monotonically increasing with V_{GS}, so the vertical order of the gain will be followed in Signature 1 in Figure 32. However, the $\Delta V_{OUT_{TS}}$ voltage variations can be too small to be significant if the right P_{IN} is taken close to $P_{IN} = -20dBm$ or too large and out of the sensor linear voltage region for $P_{IN} - 6dBm$. All

possible values of right P_{IN} are represented in Figure 33. A wide range of horizontal $\Delta V_{OUT_{TS}}$ is an important criterion, since noise and power dissipation subfolding affects the voltage measurement in the temperature sensor.

BX8: Signature 1 computes in post-processing all versions of Signature 1 with the right P_{IN} so they can be compared. $P_{IN} = [-20, -10]dBm$ was chosen as shown in Figure 32 for having the most monotonically ordered horizontal distribution of $\Delta V_{OUT_{TS}}$.

The linear fitting of Signature 1 with $P_{IN} = [-20, -10]dBm$ for the 11 ICs is shown in Figure 34, with the slopes k_1 and intercepts C represented visually in Figure 35 and numerically in Table 5. The slope k_1 has a high relative variance comparing the 11 ICs measured, but the signatures can be calibrated for each particular chip. The measured $\Delta V_{OUT_{TS}}$ ranges are similar, so Signature 1 can be a consistent gain signature.

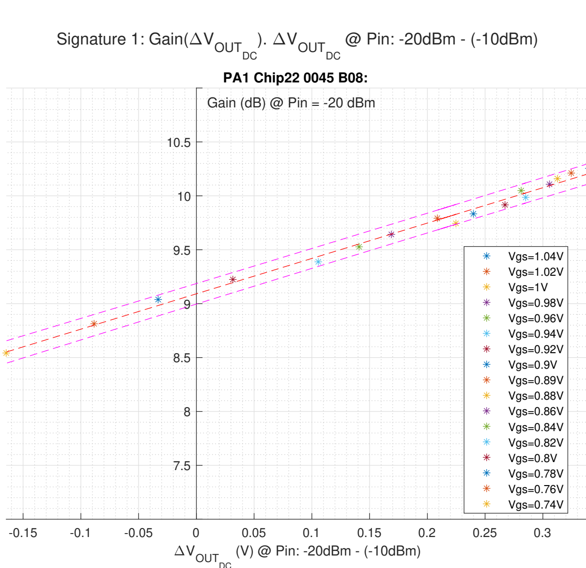

Figure 32: Signature 1 of TS 1 (PA 1), measured at $P_{IN} = [-20, -10]dBm$ for chip 22.

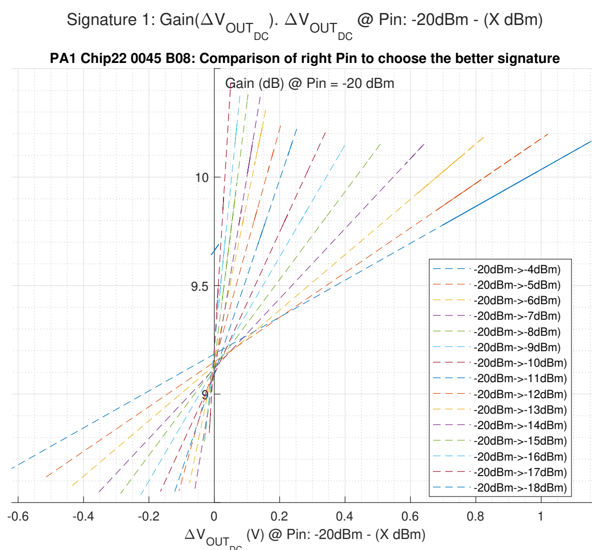

Figure 33: Shape of the linear fitting of Signature 1 for different values of right P_{IN} with left $P_{IN} = -20dBm$ for TS 1 (PA 1).

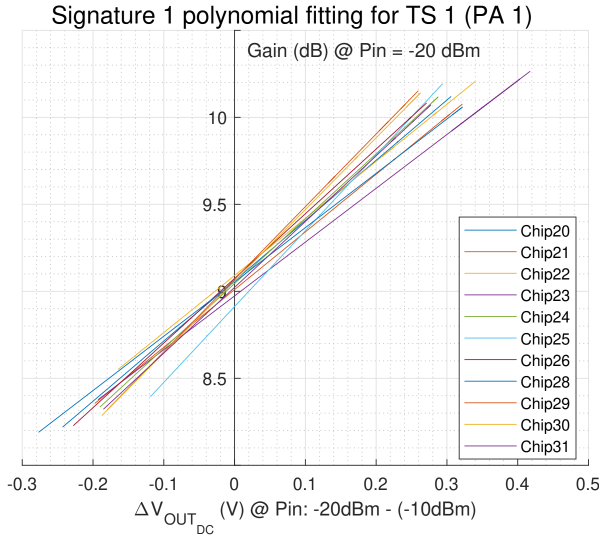

Figure 34: Comparison of linear fitting of Signature 1 of TS 1 (PA 1) for 11 ICs.

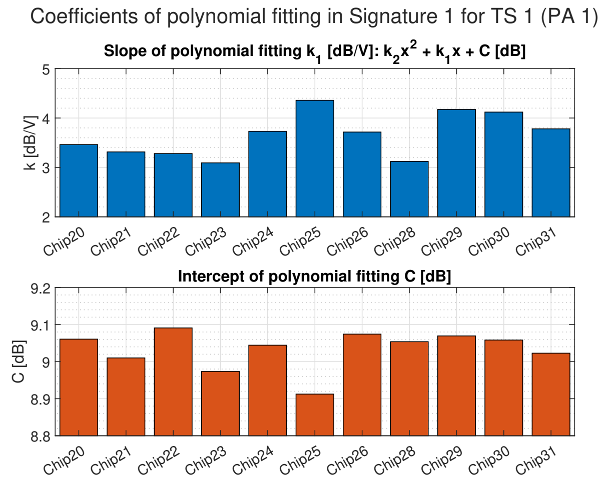

Figure 35: Coefficients of polynomial fitting of proposed Signature 1 of TS 1 (PA 1) for 11 ICs.

5.3.1.2 Signature 2a: $Gain(\Delta N)$; $N@P_{IN} = [-5, 5]dBm$ BX5: Signature 2 (2a and 2b) is divided in two variants of proposed signatures, 2a ($Gain(\Delta N)$) and 2b($I_D(\Delta N)$). Signature 2a uses a ΔN with right and left $P_{IN} = [-5, 5]dBm$, while Signature 2b uses a ΔN with right and left $P_{IN} = [OFF, -20]dBm$.

Signatures 2a and 2b use the temperature sensor DAC central N chosen for each measurement so that $V_{OUT_{TS}} = \frac{V_{DD}}{2} = \frac{3.3V}{2} = 1.65V$, as seen in Figure 36. The selected RF input power for Signature 2a is chosen $P_{IN} = [-5, 5]dBm$ where the dissipated power subfolding is very visible and maximizes the measured range ΔN. The curve fitting for the gain in Signature 2a of chip 22 is shown in Figure 37, and for the 11 ICs measured in Figure 38. The polynomial characteristics of the curve fitting for the 11 measured ICs are displayed in Figure 39 and numerically in Table 5.

Compared to Signature 1, Signature 2a has more error in the curve fitting, but the ΔN measured values are more spaces and all monotonic despite being in the region most affected by the power dissipation subfolding.

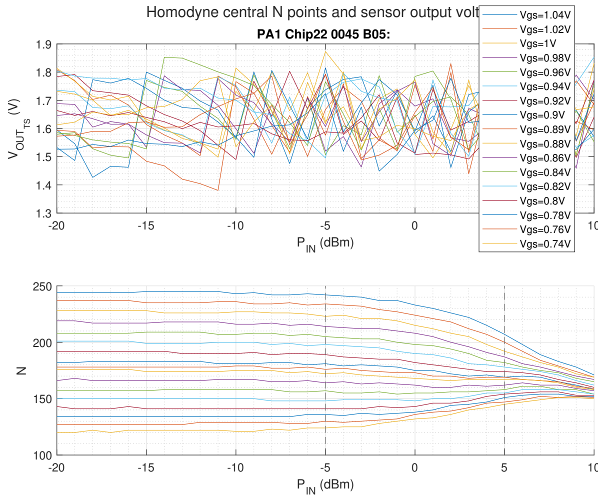

Figure 36: Features used in Signatures 2a and 2b of TS 1 (PA 1) for IC 22, measured at $P_{IN} = [-5, 5]$ dB.

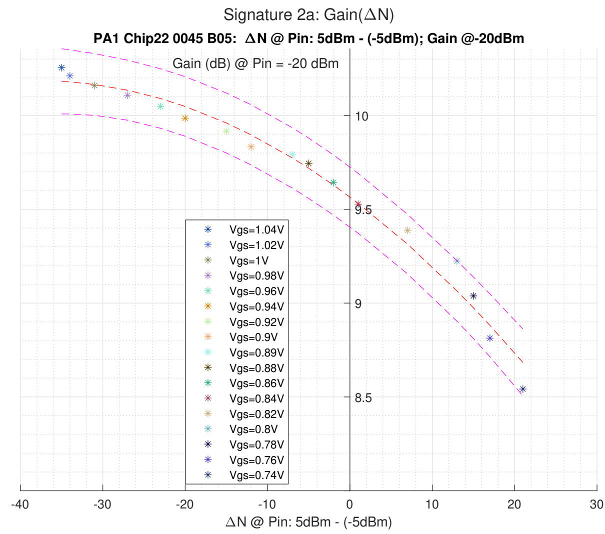

Figure 37: Signature 2a of TS 1 (PA 1) for IC 22.

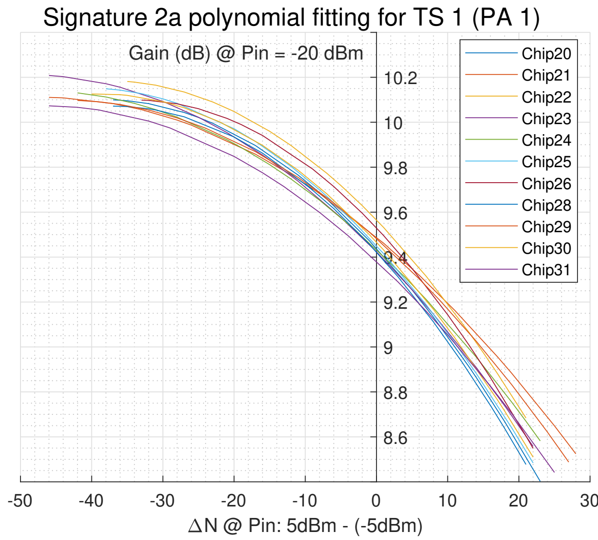

Figure 38: Comparison of polynomial fitting of Signature 2a of TS 1 (PA 1) for 11 ICs.

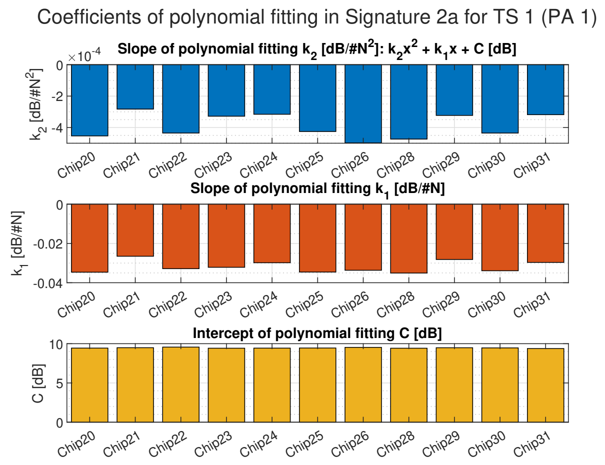

Figure 39: Proposed Signature 2a for TS 1 (PA 1).

5.3.1.3 Signature 2b: $Gain(\Delta N)$ and $I_D(\Delta N)$; $N@P_{IN} = [OFF, -20]dBm$

Signature 2b also uses the DAC central N as a signature of the gain, but taken at values of $P_{IN} = [OFF, -20dBm]$, which is the DC thermal coupling from biasing expressed in Table 4.

The curve fitting for the $I_{D_{DC}}$ and $Gain$ in Signature 2b of chip 22 is shown in Figure 40, and for the 11 ICs measured in Figure 41. The polynomial characteristics of the curve fittings for the 11 measured ICs are displayed in Figures 42 and 43 and numerically in Table 5.

Signatures 2b $I_{D_{DC}}$ and $Gain$ show very good variances for a very wide range of ΔN that corresponds to the DC thermal coupling from biasing.

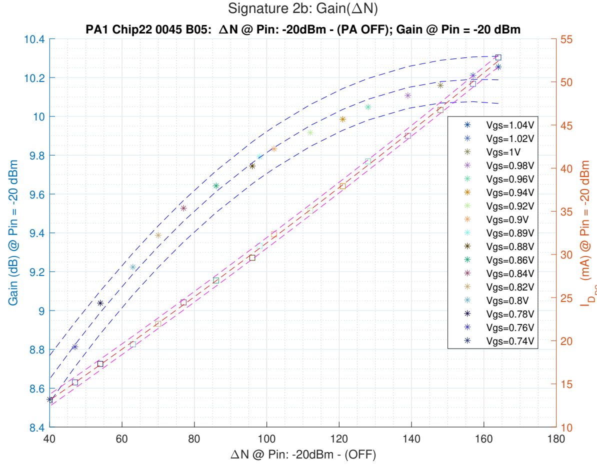

Figure 40: Scatter plot and polynomial fitting Signature 2b $Gain(\Delta N)$ and $I_D(\Delta N)$; $N@P_{IN} = [OFF, -20dBm]$ for TS 1 (PA 1) for IC 22.

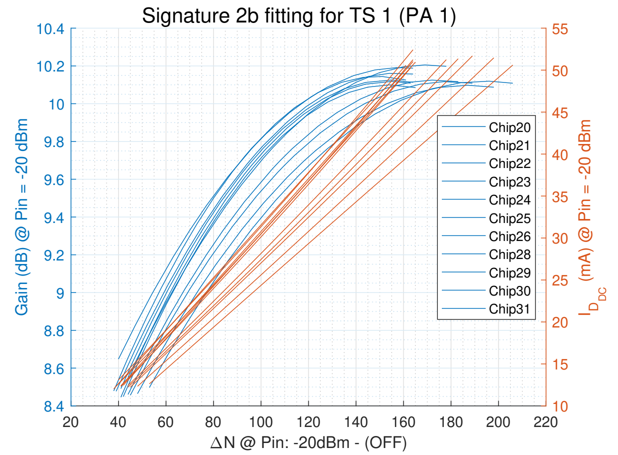

Figure 41: Comparison of polynomial fittings of Signature 2b for TS 1 (PA 1) for 11 ICs.

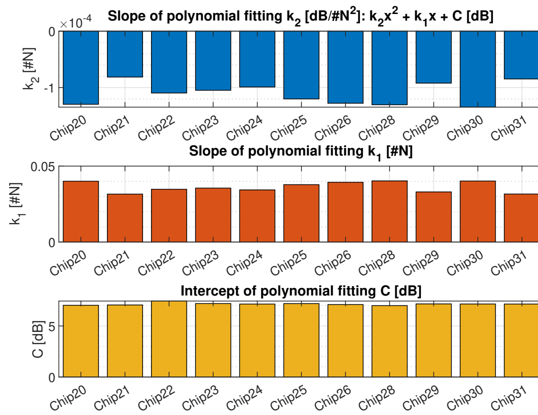

Figure 42: Coefficients of polynomial fitting of proposed Signature 2b $Gain(\Delta N)$; $N@P_{IN} = [OFF, -20dBm]$ of TS 1 (PA 1) for 11 ICs.

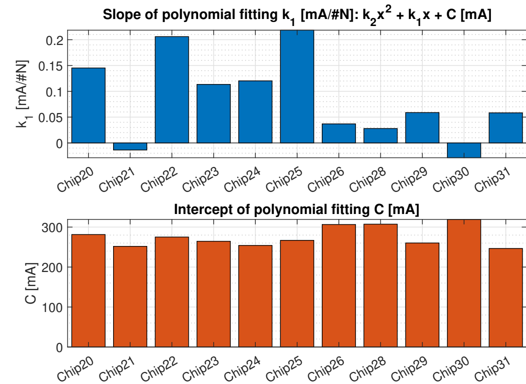

Figure 43: Coefficients of polynomial fitting of proposed Signature 2b $I_D(\Delta N)$; $N@P_{IN} = [OFF, -20dBm]$ of TS 1 (PA 1) for 11 ICs.

5.3.2 Heterodyne gain signatures

CX4: Signatures 3 and 4. The heterodyne gain signatures should not be so affected by the noise and DC levels from biasing that are intrinsic in homodyne measurements. The Lock-in $V_{OUT_{TS}Lock-in}$ measurements have very narrow bandwidth BW and show the Δf intermodulation product AC voltage in the temperature sensor as LPF filter done by the thermal coupling in Figure 2 has allowed to reach the TS.

The right Δf must be chosen to measure $V_{OUT_{TS}Lock-in}$ close to the Lock-in range of 1V so that the noise rejection is higher. The smaller the Δf, the higher the $V_{OUT_{TS}Lock-in}$. In the lab experiments, $\Delta f = 10.013MHz$ was the best value for the TS 1 bias $V_{SEN1b} = 2.5V$. The output power measurements in heterodyne when the PA is biased with two tones were noisy due to

the instrument used, so the P_{OUT} and gain were extracted from the RF characterization of the PA in Section **??**.

An interesting characteristic of $V_{OUT_{TS}Lock-in}(Gain)$ for different P_{IN} is shown in Figure 44, with the same characteristic for different V_{GS} is shown in Figure 45. Gain signatures for known P_{IN} or V_{GS} could be extracted from them, but there are better options.

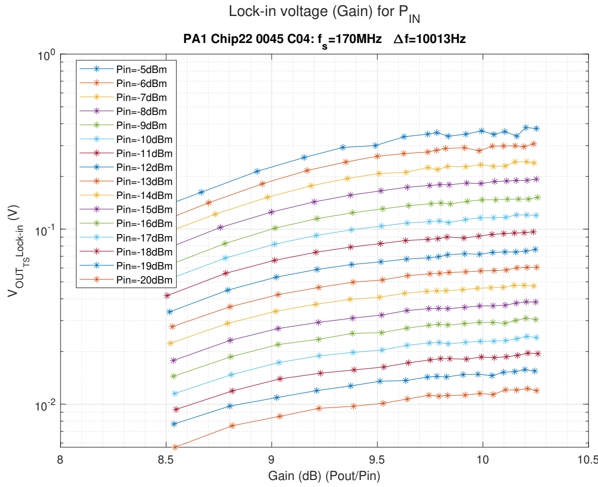

Figure 44: Heterodyne characteristics $V_{OUT_{TS}Lock-in}(Gain)$ for different P_{IN} of TS 1 (PA 1) for IC 22.

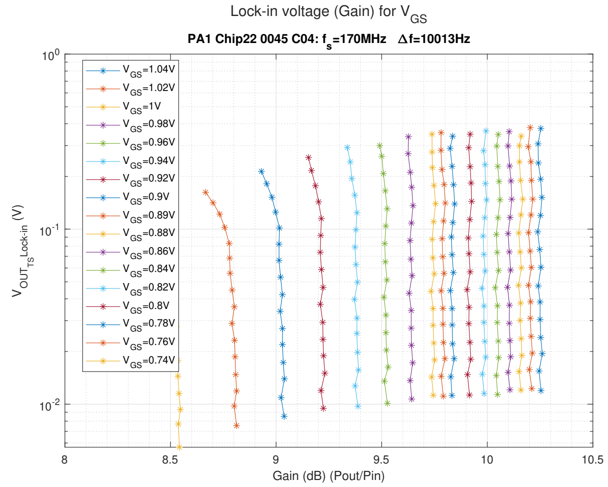

Figure 45: Heterodyne characteristics $V_{OUT_{TS}Lock-in}(Gain)$ for different V_{GS} of TS 1 (PA 1) for IC 22.

5.3.2.1 Signature 3: $Gain(slope\ log(V_{OUT_{TS}Lock-in}) - kP_{IN})$

Signature 3 uses an interesting property of the aforementioned characteristics. The 10log of the $V_{OUT_{TS}Lock-in}$ has an almost quadratic relation with the input RF power P_{IN}. This means that the slope of the $log(V_{OUT_{TS}Lock-in}) - kP_{IN}$, being k the correcting factor of measured mean $k = 2.2$, can be made flat and compact. This relation forming a flat, compact line holds for $P_{IN} = [-20, -15]dBm$.

The proposed Signature 3 can be seen in Figure 46 where the different points for each V_{GS} are the measured in $log(V_{OUT_{TS}Lock-in}) - kP_{IN}$ for $P_{IN} = [-20, -15]dBm$, with curve fitting. The same signature can be seen represented as maximum and minimum error bars in Figure 47. The curve fitting for the 11 ICs measured is displayed in Figure 48 and their polynomial coefficients in Figure 49 and in numerical form in Table 5.

The signature curve fitting is very promising on an individual level, although the intercept C is very different for half of the chips measured. This means that this signature can be used and calibrated for each chip, and used as a heterodyne gain signature.

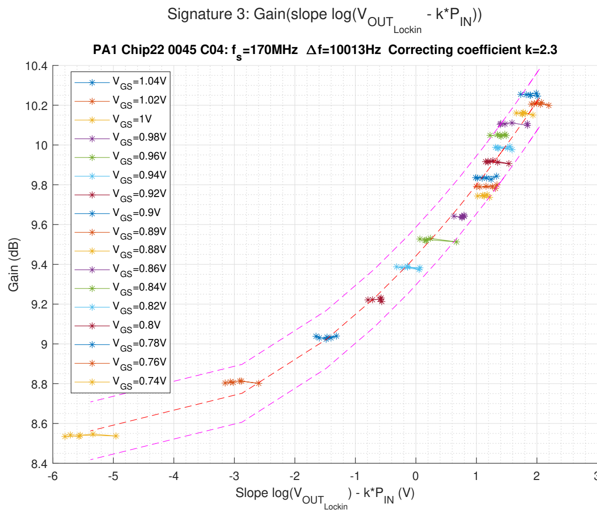

Figure 46: Scatter plot and polynomial fitting of Signature 3 of TS 1 (PA 1) for IC 22.

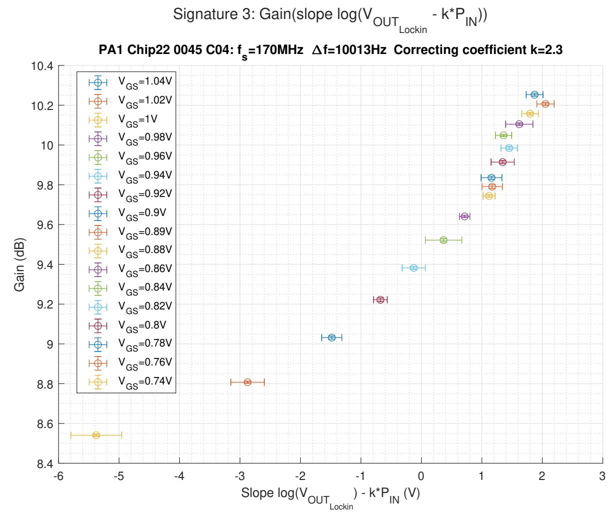

Figure 47: Proposed Signature 3 ranges of TS 1 (PA 1) for IC 22.

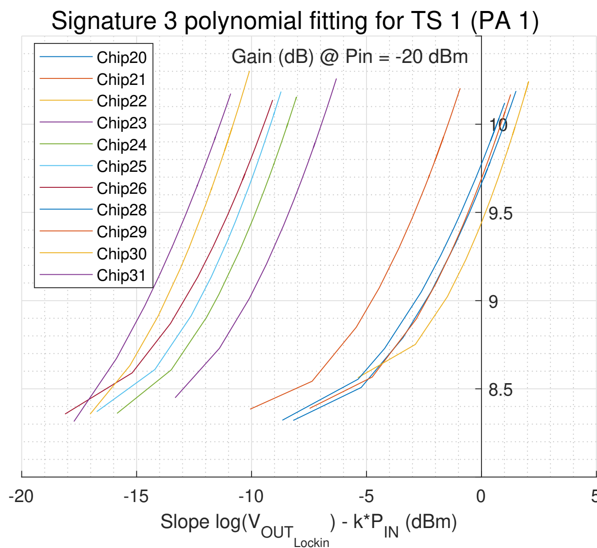

Figure 48: Comparison of polynomial fittings of Signature 3 of TS 1 (PA 1) for 11 ICs.

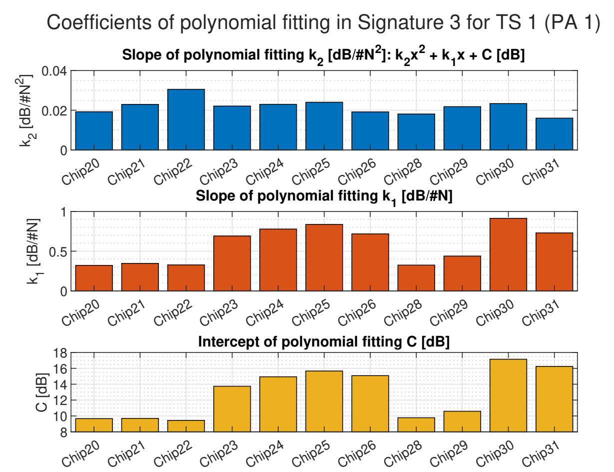

Figure 49: Coefficients of polynomial fitting of proposed Signature 3 of TS 1 (PA 1) for 11 ICs.

5.3.2.2 Signature 4: $P_{OUT}(slope\ log(V_{OUT_{TS}Lock-in}) - kP_{IN},);\ N@P_{IN} = [OFF, -20dBm]$
The same $slope\ log(V_{OUT_{TS}Lock-in})$ encountered in Signature 3 can be represented with the P_{OUT} and the DC thermal coupling as a measurement of $);\ N@P_{IN} = [OFF, -20dBm]$, as seen in Table [4].

Signature 4 forms a 3D inclined plane formed by the DC thermal coupling $);\ N@P_{IN} = [OFF, -20dBm]$ with P_{OUT} as with the homodyne Signature 2b and with extra height given by the heterodyne $slope\ log(V_{OUT_{TS}Lock-in})$ measured.

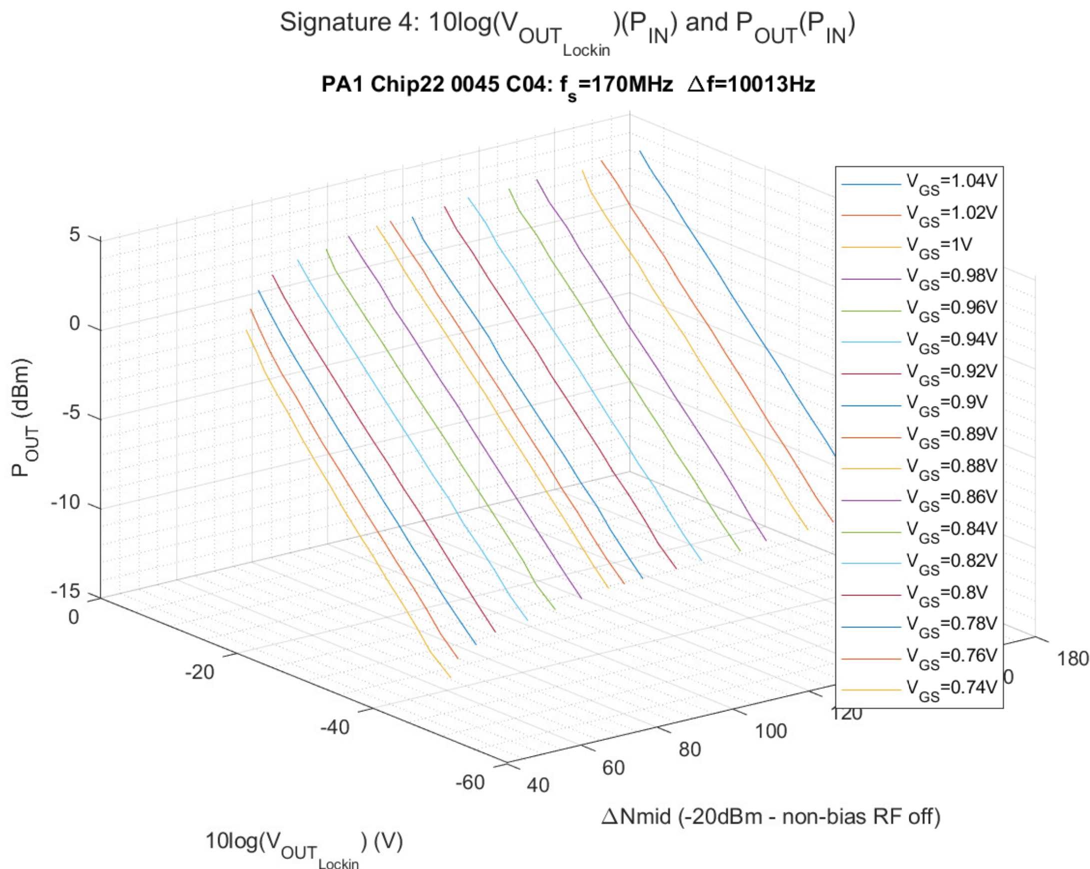

Figure 50: Signature 4 of TS 1 (PA 1) for IC 22.

5.4 Conclusions on the proposed gain signatures

The usage of the measured $V_{OUT_{TS}}$ in Signature 1, having a much smaller range to the DAC N used in Signature 2 and Signature 4, can make it more impractical or less accurate. The heterodyne gain Signature 3 can be further modeled to be used in the post-Aging recalibration.

Using signatures without calibrating the instruments and also calibrating to the individual TS characteristics of each IC is prone to uncertainties. By only having a temperature Signature on an untested IC, it is not possible to precisely monitor its gain. This can be done in further work and even directly in the Aging process, using the signatures before the Aging to correct the gain loss after the aging without even characterizing the gain.

Both homodyne and heterodyne gain signatures show promise as estimators of the power amplifier gain from indirect temperature measurements. Homodyne procedures had been deemed too noisy and with a DC thermal coupling too high relative to the variations related to the RF signal DC thermal coupling contribution, but the homodyne gain signatures show promise and are not to be discarded. Signature 4 or a variation of it could be a good combination of the Lock-in and N measurements to allow recalibration post-aging.

All characteristics and signatures are automatically generated by the post-processing programs developed in the thesis, so small changes in the signature code allow for different visualizations

of the saved measurements.

The following Table 5 contains the detailed statistics of the curve fitting of the proposed signatures measured on the 11 ICs in the laboratory.

Signatures Measured variable	Sig 1 $V_{OUT_{TS}}$	Sig 2a N	Sig 2b $Gain$ N	Sig 2b $I_{D_{DC}}$ N	Sig 3 N
k_2	0	0	-0.10992E-3	0	0.02095
Variance σ^2	0	0	406.49E-12	0	24.000e-06
Standard deviation σ	0	0	20.162E-06	0	0.00490
k_1	3.6707	-0.02514	0.03612	3.6707	0.55567
Variance σ^2	0.17937	5.5566E-06	13.254E-06	0.17937	0.04550
Standard deviation σ	0.42352	0.00236	0.00364	0.42352	0.21331
C [dB]	9.0421	9.3373	7.1482	9.0421	12.589
Variance σ^2 [dB]	0.00305	0.00256	0.01296	0.00305	7.0425
Standard deviation σ [dB]	0.05522	0.05056	0.11384	0.05522	2.6538

Table 5: Fitting parameters of the TS 1 (PA 1) signatures for 11 chips measured.

Conclusions and future work

This thesis has achieved its goal of Experimental monitoring of the gain in RF PAs using Temperature Measurements by proposing gain signatures and studying their statistics. The signatures use both homodyne and heterodyne procedures proposed by the previous work, so the analysis and implementation can be further developed in the TOGETHER project using the PAAGEANT IC.

Optimal experimental parameters such as the PA RF base frequency f_s, the biasing for the temperature sensor V_{SEN1b} or heterodyne difference frequency Δf have been studied in the laboratory, and are suggested to be used in further studies.

The thesis has even studied and measured the temperature sensor TS 2 (PA 2), but it presents behavior different enough when trying the best biasing to grant further research. Also, including those differences would compromise the clarity of this thesis memory that attempts to present the gain signatures from temperature measurements.

The measurements with TS 2 (PA 2) have been performed with and without PS biasing, to also compare and try detecting the effect of the PS, with several biasing options so that the study for TS can be continued. The programs developed in this thesis already measure TS 1 or TS 2 without effort by the laboratory staff and the programs automatically post-process and generate all the data and figures presented in this thesis memory.

Finding optimal experimental parameters for TS 2 and comparing the signatures obtained with both temperature sensors and with and without power sensor PS biasing is the next logical step in the experimental development of the project.

After that, the Aging code can be very easily integrated to the automated programs developed in this thesis and all characteristics and signatures can be compared. The Aging experiments are feasible to be performed in the next study on the project.

Acknowledgements

This Master's Thesis would not have been possible without the previous work and testing implementation on the PAAGEANT IC to characterize and recalibrate Aging with temperature measurements. I am proud to have a part in the ongoing project and hope that the automated laboratory programs I have developed during the thesis are useful in further research in the project.

The guidance, readily availability and patience from professors and tutors Josep Altet and Diego Mateo have been key in my understanding of the inner designs of the PAAGEANT IC, instruments and theory whenever I needed help with.

Also, the support, flexibility and understanding from my fellow workmates in Bleta during the thesis development have been more than generous and helped much in the personal area.

Thanks again to all those who made this project possible.

Bibliography

[1] Barajas, E.; Aragones, X.; Mateo, D.; Altet, J., DOI: 10.3390/s19214815 *Differential Temperature Sensors: Review of Applications in the Test and Characterization of Circuits, Usage and Design Methodology*, Sensors 2019, 19, 4815
Consulted *10/09/2021*

[2] Altet, J.; Mateo, D.; Silva-Martinez, J., DOI: 10.1109/MWSCAS.2014.6908606 *Embedded Temperature Sensors to characterize RF and mmW analog circuits*, Sensors 2019, 19, 4815
Consulted *11/09/2021*

[3] Altet, J.; González, J.L.; Gómez, D.; Perpiñà, X.; Claeys, W.; Grauby, S.; Dufis, C.; Vellvehi, M.; Mateo, D.; Reverter, F.; et al, DOI: 10.1016/j.mejo.2014.02.009 *Electro-thermal characterization of a differential temperature sensor in a 65 nm CMOS IC: Applications to gain monitoring in RF amplifiers*, Microelectron. J 2014, 45, 484–490
Consulted *15/09/2021*

[4] Antonin Le Miére, *Test et caractérisations de circuits analogiques souffrants de vieillissement électrique*, Master's Thesis. Universitat Politècnica de Catalunya, Grenoble INP Phelma, 2019
Consulted *22/09/2021*

[5] Marçal Olivé i Muñiz, *Caracterització experimental de circuits RF basada en sensors integrats*, Bachelor Thesis. Universitat Politècnica de Catalunya, ETSETB, 2020
Consulted *20/09/2021*